CHALMERS

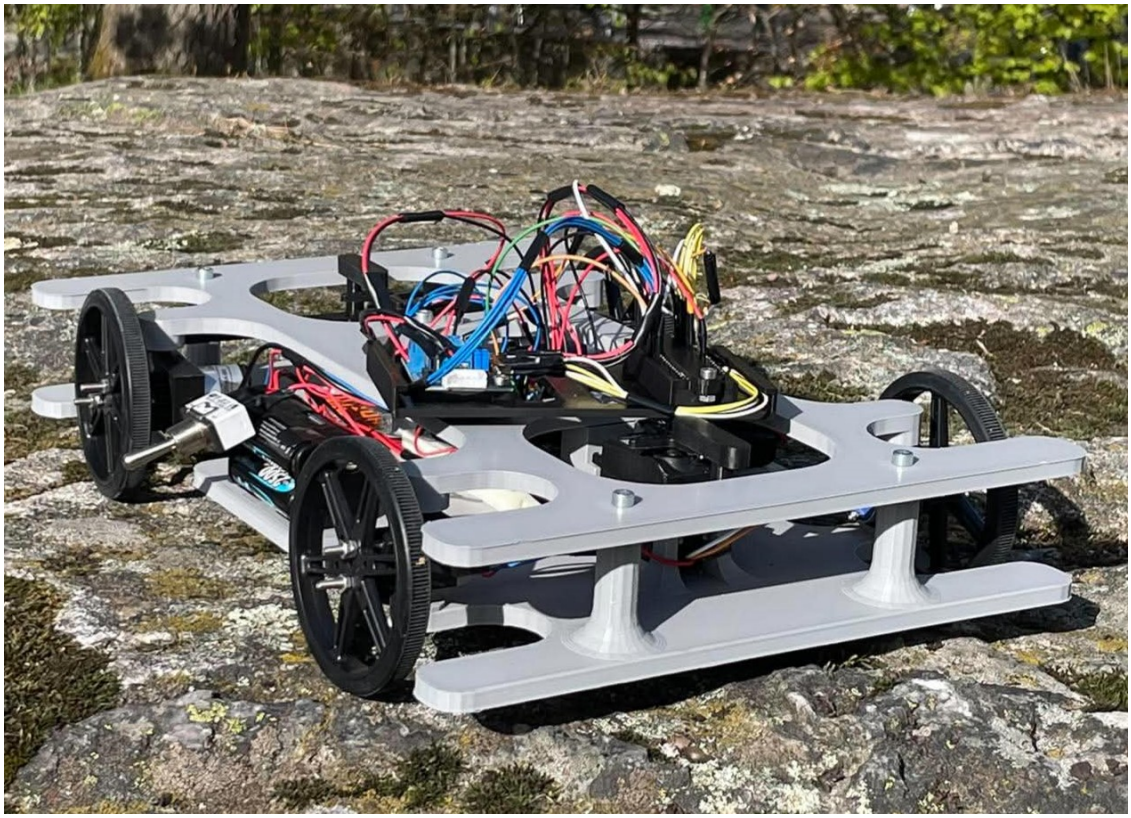

Development and testing of a steer-by-wire platform, using a four-wheel steering control system

A study on how prototype vehicles can be used to evaluate steering control strategies

Bachelor's thesis in Electrical Engineering

Anders Frick, Valter Isaksson, Amar Omanovic

DEPARTMENT OF ELECTRICAL ENGINEERING
DIVISION OF SYSTEMS AND CONTROL

CHALMERS UNIVERSITY OF TECHNOLOGY
Gothenburg, Sweden 2026
www.chalmers.se

Bachelor's thesis 2026

Development and testing of a steer-by-wire platform, using a four-wheel steering control system

A study on how prototype vehicles can be used to evaluate steering control strategies

Anders Frick, Valter Isaksson, Amar Omanovic

CHALMERS

Department of Electrical Engineering
Division of Systems and Control
EENX16-VT26-10
Chalmers University of Technology
Gothenburg, Sweden 2026

Development and testing of a steer-by wire control system for four-wheel steering
A study on how prototype vehicles can be used to evaluate steering control strategies
Anders Frick, Amar Omanovic, Valter Isaksson

Supervisor: Wenliang Zhang, Department of Electrical Engineering
Examiner: Nikolce Murgovski, Department of Electrical Engineering

Bachelor's Thesis 2026
Department of Electrical Engineering
Division of Systems and Control
EENX16-VT26-10
Chalmers University of Technology
SE-412 96 Gothenburg
Telephone +46 31 772 1000

Typeset in LaTeX
Gothenburg, Sweden 2026

Abstract

The rapid electrification of the automotive industry has created new opportunities for integrated vehicle control, including steer-by-wire and four-wheel steering systems. Small-scale prototypes can provide a cost-effective platform for developing and evaluating control strategies aimed at improving vehicle stability and maneuverability. The purpose of this project was to design, assemble, and evaluate a small-scale electric vehicle prototype equipped with electronically actuated four-wheel steering to investigate vehicle dynamics and path-following control. A modular chassis was developed using 3D-printed components, integrating two DC propulsion motors, two steering servos, and a Teensy 4.1 microcontroller. A Proportional–Integral (PI) control strategy was implemented in simulation to regulate wheel speed and steering angle. Due to hardware-related and time constraints, the physical implementation was limited to individual PI-based wheel speed regulation. Testing demonstrated that the PI controllers successfully maintained the target average wheel speed of 80 RPM with a small mean error. However, the physical tests revealed that instantaneous speed variations, amplified by sensor noise and mechanical tolerances in the 3D-printed assemblies, introduced lateral instability and deviations from a straight path. Ultimately the project delivered a simulation using a PI control strategy and a hardware platform for further four-wheel steering research.

Nomenclature

$\ddot{\psi}$	Change in yaw rate $[\frac{rad}{s^2}]$
δ	Wheel steering angle [rad]
δ_{max}	Maximum wheel steering angle [rad]
$\dot{v}_j$	Acceleration along local axis j$\in${x,y} $[\frac{m}{s^2}]$
$\dot{X}$	Vehicle velocity along global x-axis $[\frac{m}{s}]$
$\dot{Y}$	Vehicle velocity along global y-axis $[\frac{m}{s}]$
$\dot{\omega}_i$	Change in angular velocity for wheel i$\in${fl,fr,rl,rr} $[\frac{rad}{s^2}]$
$\dot{\psi}$	Yaw rate $[\frac{rad}{s}]$
μ	Friction constant [-]
ω_h	Angular velocity along vehicle path curve h$\in${c,equal} $[\frac{rad}{s}]$
ω_{max}	Maximum angular velocity for DC-motors $[\frac{rad}{s}]$
ω_{rated}	Rated angular velocity for DC-motors $[\frac{rad}{s}]$
ψ	Yaw angle [rad]
a	Assumed acceleration $[\frac{m}{s^2}]$
B	Vehicle track width [m]

b_f Distance from vehicle symmetry line to front left wheel [m]

b_r Distance from vehicle symmetry line to rear left wheel [m]

C_α Tyre cornering stiffness $[\frac{N}{rad}]$

C_κ Tyre longitudinal stiffness [N]

C_{rr} Rolling resistance coefficient [-]

e Difference between target value and current value (unit depends on regulator configuration)

e_D Derivative difference between target value and current value over time (unit depends on regulator configuration)

e_I Integrated difference between target value and current value over time (unit depends on regulator configuration)

F_{xi} Force for wheel i$\in${fl,fr,rl,rr} in the wheels forward direction [N]

F_{yi} Force for wheel i$\in${fl,fr,rl,rr} in the wheels horizontal direction [N]

g Gravitational acceleration $[\frac{m}{s^2}]$

h Simulation time step [s]

h_g Distance from ground to center of gravity [m]

I_z Z-axis inertia around vehicle center of gravity [kgm^2]

I_{wheel} Wheel rotation inertia [kgm^2]

K_D Regulation derivative parameter (unit depends on regulator configuration)

K_I Regulation integrating parameter (unit depends on regulator configuration)

K_P Regulation proportional parameter (unit depends on regulator configuration)

K_{max} Regulation critical gain (unit depends on regulator configuration)

L Vehicle wheelbase [m]

l_f Distance from center of gravity to front axle [m]

l_r Distance from center of gravity to rear axle [m]

L_{veh} Length of vehicle [m]

m Vehicle mass [kg]

m_ω Wheel mass [kg]

m_{est} Estimated total vehicle mass [kg]

n Number of propulsion motors[-]

P_{max} Maximum DC-motor effect [W]

r Wheel radius [m]

r_p Radius of path curve p$\in${c,l,r} [m]

T_0 Regulation period of oscillation during critical gain [s]

T_i Torque affecting wheel i$\in${fl,fr,rl,rr} [Nm]

T_{max} Maximum torque for DC-motors [Nm]

T_{motor} Required torque per motor [Nm]

T_{rated} Rated torque for DC-motors [Nm]

$T_{req,final}$ Actual required torque per motor [Nm]

T_{sensor} Added sensor mechanical load [Nm]

u Regulation control signal (unit depends on regulator configuration)

v_j Velocity along local axis j$\in${x,y} [$\frac{m}{s}$]

v_k	Velocity of path curve k∈{c,l,r,in,out} $[\frac{m}{s}]$
W_{veh}	Width of vehicle [m]
X	Systems global x-axis [m]
x	Vehicle's local x-axis, pointing in forward vehicle direction [m]
Y	Systems global y-axis [m]
y	Vehicle's local y-axis, pointing in left horizontal vehicle direction [m]

List of Acronyms

The list of acronyms used through this project is listed below in alphabetic order:

CAD	Computer-Aided Design
DC	Direct Current
DC/DC	Direct Current to Direct Current
IMU	Inertial Measurement Unit
MPC	Model Predictive Control
NiZn	Nickel–Zinc
PETG	Polyethylene Terephthalate Glycol
PI	Proportional–Integral
PID	Proportional–Integral–Derivative
PLA	Polylactic Acid
PWM	Pulse Width Modulation
RC	Radio Control
RPM	Revolutions Per Minute
SEK	Swedish Krona

Contents

1 Introduction **1**
- 1.1 Purpose and Aim . . . 2
- 1.2 Limitations and delimitations . . . 2

2 Theory **4**
- 2.1 Stability . . . 4
- 2.2 Overview of turning dynamics . . . 5
  - 2.2.1 Turning dynamics - solid axles . . . 5
  - 2.2.2 Turning dynamics - separate wheels . . . 7
  - 2.2.3 Turning dynamics - Ackermann steering with separate wheels 10
- 2.3 Mathematical modeling of vehicle dynamics . . . 10
- 2.4 Overview of regulation . . . 12
  - 2.4.1 PI regulator . . . 12
  - 2.4.2 PID regulator . . . 12
  - 2.4.3 MPC regulator . . . 13

3 Implementation **14**
- 3.1 Turning dynamics . . . 14
- 3.2 Regulators . . . 15
- 3.3 Implementation of PI regulation . . . 16

4 Components Selection **18**
- 4.1 Propulsion motors . . . 18
- 4.2 Motor driver . . . 19
- 4.3 Rotary position sensors . . . 20
- 4.4 Steering motors . . . 20
- 4.5 Microcontroller . . . 20
- 4.6 IMU . . . 20
- 4.7 Batteries . . . 21
- 4.8 Power supply stabilization . . . 21

5 Development of Vehicle Platform **22**
- 5.1 Development of the physical vehicle prototype . . . 23
- 5.2 Mechanical design components . . . 24
- 5.3 Electrical integration . . . 27

5.4 Relevant Simulation Parameters 29
5.5 Control software implementation 30

6 Results and Discussion **33**
6.1 Turning Dynamics Simulation 33
6.2 Discussion of Turning Dynamics Results 34
6.3 PI Controller Simulations 35
6.3.1 Velocity Control 35
6.3.2 Driving Without Steering 38
6.3.3 Steering Control 40
6.4 Discussion of Simulation Results 41
6.5 Physical Prototype Wheel Speed Regulation 43
6.5.1 Physical prototype lane-keeping test 44
6.5.2 Discussion of Physical Prototype Results 45

7 Conclusion **47**
References 48

A Appendix **51**
A.1 Additional prototype images 51

List of Figures

2.1 The image illustrates the paths taken by the wheels of a vehicle along with important variables. . . . 6
2.2 The image illustrates the paths taken by the wheels of a vehicle along with important variables. . . . 8
2.3 The image illustrates the variables defining the vehicle model. . . . 11

4.1 Overview of electrical system integration. . . . 21

5.1 The fully assembled prototype vehicle, from above. . . . 23
5.2 Final physical vehicle design with one steering servo per axle and two-wheel drive. Note that the prototype slightly deviates from the CAD model. . . . 24
5.3 Design of the bottom plate with its main features. . . . 25
5.4 The two housing designs. Left: motor and sensor housing for the driven wheels. Right: sensor-only housing for the non-driven wheels. . . 26
5.5 Functional electrical diagram of the vehicle, showing the power distribution, voltage regulation, control signals, and feedback signals between the main components. . . . 28
5.6 The image illustrates full/ideal PI regulation implementation for this project. . . . 32

6.1 Representation of the different speeds, during a left turn, based on the outermost wheel, according to "Turning dynamics - separate wheels". 33
6.2 Representation of the different speeds, during both left and right turns, based on the outermost wheel, according to "Turning dynamics - separate wheels". . . . 34
6.3 Representations of speed regulation when: not turning, goal is 50% of maximum velocity, K_P=0.9 , K_I≈64,86 . . . 36
6.4 Representations of speed regulation when: not turning, goal is 50% of maximum velocity, K_P=0.9 , K_I≈64,86 . . . 37
6.5 Representations of vehicle movement when regulating speed, but not steering. . . . 38
6.6 Representations of vehicle movement when regulating speed, but not steering. . . . 39
6.7 Representations of vehicle movement when regulating speed and steering. . . . 40

6.8 Representations of vehicle movement when regulating speed and steering. 41
6.9 Measured wheel speed during PI speed control of the physical prototype. The dashed line shows the target speed of 80 RPM, while the solid lines show the measured rotational speeds of the left and right wheels. 43

A.1 Side view of the assembled prototype showing the chassis layout. . . . 51
A.2 Side view of the assembled prototype from the opposite side, showing the chassis layout. 51

1

Introduction

The automotive industry has undergone significant changes in recent years, partly driven by a rapid increase in the adoption of electric vehicles, as reflected in statistics showing the increased number of electric vehicles sold each year [1]. The modern evolution of electric vehicles is of interest not only due to reduced emissions and improved efficiency, but also because of the new technological opportunities it enables.

One area significantly affected by this transition is vehicle steering. Traditional steering systems rely on mechanical linkages connecting the steering wheel to the front wheels [2]. In contrast, steer-by-wire systems replace the mechanical connection with electronic sensors, controllers, and actuators [3]. This increases design flexibility and allows the steering behavior to be controlled electronically [4].

Steer-by-wire also enables more advanced steering concepts such as four-wheel steering. By using electric actuators on both the front and rear axles, steering angles can be coordinated without complex mechanical couplings. As a result, four-wheel steering can be implemented more effectively, improving maneuverability and enhancing vehicle stability through advanced control strategies [5].

In parallel with developments in steering, electrification has also changed vehicle propulsion systems. Conventional vehicles typically rely on a single engine that distributes torque to the wheels through mechanical components, such as differentials [2]. Electrification enables alternative propulsion architectures, including multiple electric motors distributed on individual axles or wheels [6]. The propulsion and steering system could therefore be treated as part of the same control system, rather than treating them as separate subsystems.

The combination of electronically actuated steering and electric propulsion creates new possibilities for integrated vehicle control and stability. Such systems are particularly relevant in autonomous vehicle development. Autonomous vehicles rely on sensors and control algorithms to navigate without human interference and need precise vehicle control for easy maneuvering while maintaining stability and safety [7]. This makes it relevant to develop platforms where steering, propulsion, sensing, and control algorithms can be studied together.

Small-scale prototype vehicles provide a practical way to investigate these concepts. They allow control strategies to be implemented and evaluated at lower cost and risk compared to full-scale vehicles. Using prototype vehicles can therefore help to discover challenges related to hardware integration, sensor feedback and mechanical design. This motivates the development of a small-scale electric vehicle prototype with electrically actuated four-wheel steering, with the intent to investigate path-following control and steering behavior using four-wheel steering.

1.1 Purpose and Aim

The primary purpose of this bachelor thesis was to design, construct, and evaluate a small-scale, electrically actuated four-wheel steering prototype vehicle to investigate steer-by-wire control strategies and potential causes of instability. Furthermore, the study seeks to validate the theoretical control model through quantifiable physical and simulated testing. By establishing measurable performance metrics, the project aims to identify the mechanical and software limitations of the current design.

Ultimately, the thesis intends to deliver a functional, modular hardware platform and a framework for future utilization in research regarding advanced vehicle dynamics.

1.2 Limitations and delimitations

This project had several limitations that affected both the implementation and testing.

One of the main limitations was the available budget and time. The budget was limited to 5000 SEK, which affected the choice of components and required some design compromises. The available time also limited how much the design could be tested and improved. Because of this, not all control strategies, design changes, or test scenarios could be investigated within the project.

To reduce the budgetary needs, the propulsion had to be limited to implementing either front- or rear-wheel drive instead of constructing a prototype with four-wheel drive. As to further reduce the workload and implementation time, one of these driving strategies had to be overlooked. After deep consideration, front-wheel drive became the selected method of choice.

The results are also limited since the vehicle was built as a small-scale prototype. Therefore, the results should not be considered directly transferable to a full-scale vehicle without further modeling and testing. The project was also limited by the available manufacturing resources. Not all parts could be manufactured with the desired precision or material properties, which meant that some design choices had to be adapted to the tools and methods available.

To keep the mechanical design simpler, the prototype was built without a suspension

system. This made the vehicle more dependent on a flat driving surface, since uneven surfaces could affect wheel contact and sensor measurements due to vibrations. For this reason, all physical tests were performed on a flat and dry surface. This made the tests more repeatable but also means that the results are limited to relatively simple driving conditions.

2

Theory

This section presents the theoretical background needed to model, simulate and control the prototype vehicle. Firstly, a theoretical analysis defining stability is presented to serve as a basis for reasoning behind the selection of methods.

Secondly, different potential models for turning dynamics are presented, including their relationships between turning radii, angular velocities and wheel speeds. A simplified vehicle dynamics model is then presented to describe the vehicle's motion, depending on the aforementioned relationships.

Finally, different control and regulation strategies are introduced. The main focus is the potential use of the PI, Proportional–Integral, PID, Proportional–Integral-Derivative, and MPC, Model Predictive Control, regulators, respectively.

2.1 Stability

For this project, stability shall be defined as having the vehicle follow a path as close as possible without it experiencing any form of slip. According to [8], this form of vehicle stability can be obtained through making sure that two factors are contained within acceptable parameters. Those factors are the side slip angle and the yaw rate of the vehicle.

The side slip angle can be defined as the number of degrees between the vehicle's current orientation vector and the direction in which the velocity vector is pointing. The goal is to have the side slip angle be as close to zero as possible, since that would mean that the car is only driving in its direction of orientation, and not horizontally.

The yaw rate is the speed at which the vehicle rotates around its center of mass. Having zero yaw rate means that the vehicle is not turning, too high yaw rate means that it is spinning, but just enough yaw rate means that it is turning.

It should also be noted that both variables have limiting boundaries, which should be implemented to make sure that they remain acceptable to the point that vehicle stability is preserved. Their boundaries are set as described in [8].

2.2 Overview of turning dynamics

In the case that a car turns without stopping and without alternating the steering angle, it may follow a pattern closely resembling a circle, meaning that it should return to the position in which it has started. That circle will have its own radius (r_c) and rough center point of which the car revolves around.

When it comes to circular motion, if an object revolves around a central point and performs a full loop within a specific time, then that object has an angular velocity (ω_c). If the object's angular velocity remains the same, but the radius from the central point changes, then the vehicle's actual velocity (v_c) may also change. The relation can be described as

$$\omega_c = \frac{v_c}{r_c} \tag{2.1}$$

This indicates that the object's speed should increase or decrease with the radius.

A car is not a singular point. If a car were to drive in a circle, some wheels should be closer to the central point of the turn. Therefore, the wheels should be driven at different speeds if a constant angular velocity is to be preserved. However, the distance from the center point to each wheel should be considered dynamic since it may change at any time, and the distance may vary based on how the vehicle is built to steer.

One possible way to negate having to account for this is by using a differential, which, according to [9], allows for the wheels of an axle to move at different speeds without the use of multiple motors. However, based on factors such as the number of motors and budgetary variables, alternative solutions may be more viable and even optimal to use.

In theory, having motors directly connected to the wheels in question could likely result in the wheel velocities being more responsive to change when needed. If they are more responsive, then it could be a great source for stability since the two aforementioned stability parameters can be more effective and quicker regarding implementation and regulation within the set boundaries.

Therefore, the following sections shall analyze different solutions for turning based on the facts previously stated in the theory and in the introduction.

2.2.1 Turning dynamics - solid axles

One possible solution for the turning would be having each wheel turning with its corresponding axle as shown in Figure 2.1. Considering that the vehicle shall be using four-wheel steering, the easiest way to construct this solution would be having the rear wheel axle turn towards the opposite angle of the front wheel axle. This would result in the front and rear axles being rough mirror images of each other

during movement. Therefore, the inner wheels should follow the same path while the outer wheels follow their path, as previously illustrated.

The result of this would be that all four wheels turn around the same central point, with the distance from that point being the varying factor. As shown in Figure 2.1, there are three different circular paths that are being followed. The first one is that of the left wheels, moving at a speed of v_l at a radius of r_l, the second one is the vehicle's actual movement along the curve, with the speed v_c at the radius of r_c, and the last one is that of the right wheels, moving with the speed v_r at a radius of r_r.

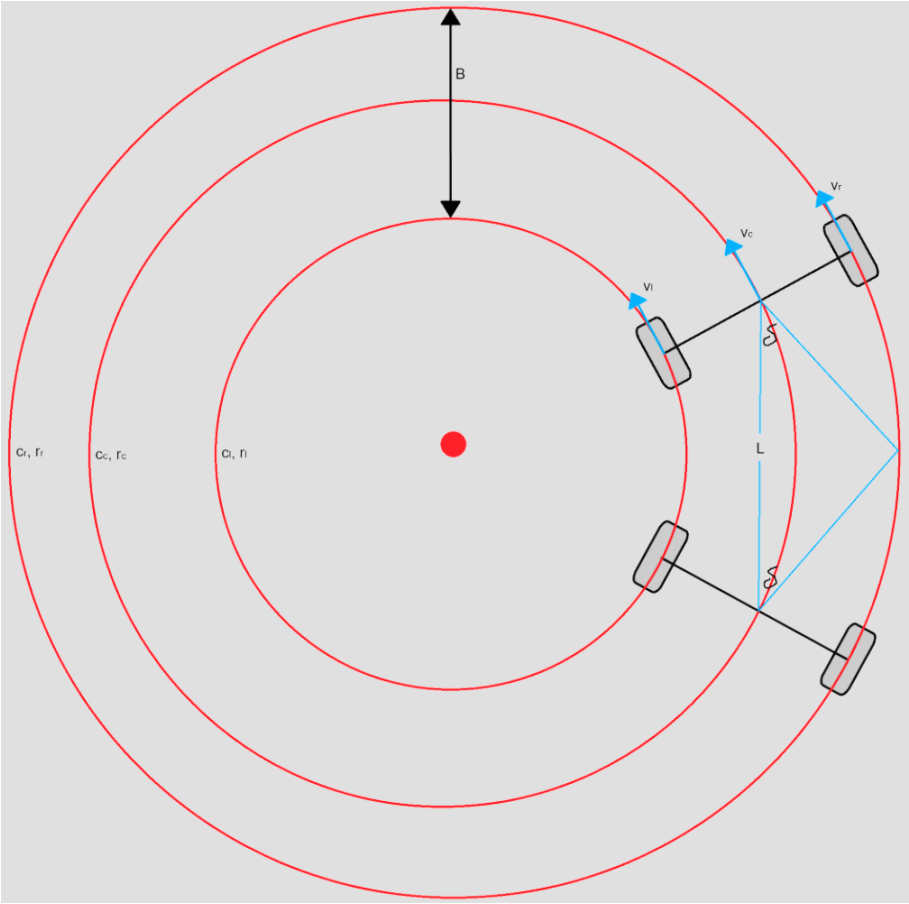

Figure 2.1: The image illustrates the paths taken by the wheels of a vehicle along with important variables.

If both axles turn at an angle with the wheelbase being defined by the variable L, then that would lead to the resulting radius being defined as

$$r_c = \frac{L}{2sin(\delta)} \tag{2.2}$$

The right wheels are positioned at a distance of half the vehicle track width from the central curve away from the central point, while the left wheels are positioned

the same distance in the opposite direction. This then gives

$$r_l = r_c - \frac{B}{2} = (\frac{L}{sin(\delta)} - B) * \frac{1}{2} \tag{2.3a}$$

$$r_r = r_c + \frac{B}{2} = (\frac{L}{sin(\delta)} + B) * \frac{1}{2} \tag{2.3b}$$

Considering that the angular velocity, as previously stated, has to be equal for all positions, that then gives

$$\omega_{equal} = \frac{v_l}{r_l} = \frac{v_c}{r_c} = \frac{v_r}{r_r} \tag{2.4}$$

Combining the previous equations gives the resulting correlations

$$v_l = v_r * \frac{L - Bsin(\delta)}{L + Bsin(\delta)} \tag{2.5a}$$

$$v_c = v_r * \frac{L}{L + Bsin(\delta)} \tag{2.5b}$$

If the vehicle were to turn it's wheels to the right, the equations would instead be

$$v_r = v_l * \frac{L - Bsin(|\delta|)}{L + Bsin(|\delta|)} \tag{2.6a}$$

$$v_c = v_l * \frac{L}{L + Bsin(|\delta|)} \tag{2.6b}$$

However, the velocity around the central curve is not the velocity of the vehicle. The speed of the vehicle can be broken down into it's x and y components. However, the goal shall almost always be to have the speed in direction y as small as possible, since pure horizontal movement from the center of mass may not be ideal. Therefore, the momentary velocity while following a curve should have a goal speed of velocity v_x in forward direction, which is tangential to the curve in this case. This then gives the relation

$$\frac{v_c}{r_c} = \frac{v_x}{r_x} = \frac{v_x}{r_c cos(|\delta|)} \Rightarrow v_x = v_c cos(|\delta|) \tag{2.7}$$

2.2.2 Turning dynamics - separate wheels

Another possible solution would be having the wheels turn independently at the edges of the axles. For the same reasons as in the previous model, it has been decided to turn each wheel the same amount of degrees. This would mean that the front wheels remain parallel to each other while the rear wheels are, practically, reflections of the front wheels.

However, as illustrated in Figure 2.2, the wheels may be parallel to each other, but do not share the same central point of rotation. This in turn means that the

methodology of calculating the speeds, for which this vehicle needs to turn properly, can not be the same as before without reformatting the problem.

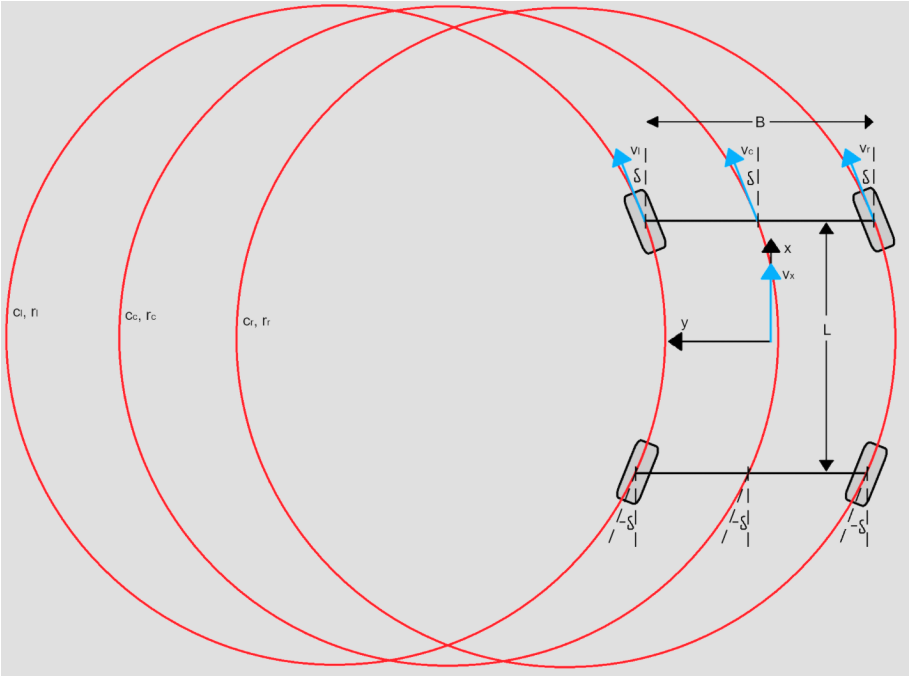

Figure 2.2: The image illustrates the paths taken by the wheels of a vehicle along with important variables.

The curve which the vehicle follows, with the radius r_c, shall be considered as the curve with the central point which every wheel will revolve around. Now, since the wheel's do not move tangentially with the angular velocity of the curve, the components of the speed have to be accounted for based on specific coordinates away from the center. Only the left turn shall be analyzed for the moment.

Firstly, the radius r_c can be described as in Equation 2.2. If the distance between the wheel's and the edge's of the solid beams is assumed to be as small as possible, meaning that the wheel is as close to the point of rotation, then that would reasonably lead to all of the radii being roughly the same.

Secondly, it can be assumed that the back wheels should affect the speed's for each track. However, since the plan is to make this prototype small in mass and volume. It is assumed that the dragging force's of the rear wheel's, which minimize the total velocity, should not be great enough as to affect the results of the following calculations, when compared to the force generated by commonly found DC-motors fitting for this project.

Thirdly, the speeds from the front wheels, v_l & v_r, can be formulated as

$$\mathbf{VL} = \begin{bmatrix} v_l * cos(\delta) \\ -v_l * sin(\delta) \end{bmatrix}_{xy} \tag{2.8a}$$

$$\mathbf{VR} = \begin{bmatrix} v_r * cos(\delta) \\ -v_r * sin(\delta) \end{bmatrix}_{xy} \tag{2.8b}$$

Lastly, the positions for the wheels need to be accounted for. However, the positions are currently based on a curve which is constantly changing. Therefore, the positions need to be dynamic. The positions for the speeds, v_l & v_r respectively, have been found to be

$$\mathbf{PL} \approx \begin{bmatrix} \frac{L}{2} \\ r_c cos(\delta) - \frac{B}{2} \end{bmatrix}_{xy} \tag{2.9a}$$

$$\mathbf{PR} \approx \begin{bmatrix} \frac{L}{2} \\ r_c cos(\delta) + \frac{B}{2} \end{bmatrix}_{xy} \tag{2.9b}$$

Using these formulated equations, one singular angular velocity can be formulated as

$$\omega_{equal} = \frac{v_c}{r_c} = \frac{(\mathbf{PL} \times \mathbf{VL})_z}{||\mathbf{PL}||^2} = \frac{(\mathbf{PR} \times \mathbf{VR})_z}{||\mathbf{PR}||^2} \tag{2.10}$$

Using the previous equations to solve Equation 2.10 gives the resulting functions

$$\begin{aligned} v_l = v_r * \frac{(Lcot(\delta) + B)cos(\delta) + Lsin(\delta)}{(Lcot(\delta) + B)^2 + L^2} \\ * \frac{(Lcot(\delta) - B)^2 + L^2}{(Lcot(\delta) - B) * cos(\delta) + L * sin(\delta)} \end{aligned} \tag{2.11a}$$

$$v_c = v_r * L \frac{(Lcot(\delta) + B)cot(\delta) + L}{(Lcot(\delta) + B)^2 + L^2} \tag{2.11b}$$

These equations come as a result of turning left. However, a vehicle such as a car has to be able to turn right. The movement and dynamics is exactly the same whether it is a right turn or a left turn. The only difference is which wheels are the inner wheels and which once are the outer wheels. Therefore, when turning right, the speed v_l instead represents the right wheel speed while v_r represents the left wheel speed. Substituting the variables instead for the speed of the inner wheel, v_{in}, and the outer wheel, v_{out} the equations now become

$$v_{in} = v_{out} * \frac{(L * cot(|\delta|) + B) * cos(|\delta|) + L * sin(|\delta|)}{(L * cot(|\delta|) + B)^2 + L^2} * \frac{(L * cot(|\delta|) - B)^2 + L^2}{(L * cot(|\delta|) - B) * cos(|\delta|) + L * sin(|\delta|)} \tag{2.12a}$$

$$v_c = v_{out} * L * \frac{(L * cot(|\delta|) + B) * cot(|\delta|) + L}{(L * cot(|\delta|) + B)^2 + L^2} \tag{2.12b}$$

Similarly to the previous model, the velocity around the central curve is not the velocity of the vehicle. Using the reasoning form the previous model, this then gives the relation

$$\frac{v_c}{r_c} = \frac{v_x}{r_x} = \frac{v_x}{r_c cos(|\delta|)} \Rightarrow v_x = v_c cos(|\delta|) \tag{2.13a}$$

$$v_x = v_{out} * cos(|\delta|) L \frac{(L * cot(|\delta|) + B) * cot(|\delta|) + L}{(L * cot(|\delta|) + B)^2 + L^2} \tag{2.13b}$$

2.2.3 Turning dynamics - Ackermann steering with separate wheels

The complexities in the previous section come from the wheels not being tangential to the central point of revolution. This can easily be fixed by steering the wheels with Ackermann steering, which means that, according to [2], all wheels are turned separate degrees as to be tangential to the central point of revolution.

2.3 Mathematical modeling of vehicle dynamics

The relationship between a vehicle's physical attributes, such as mass, and it's dynamics are different for every vehicle. To extrapolate the specific relationships between the different attributes used to calculate, for example, force and acceleration requires a mathematical model of the vehicle. The model shown in [10] is of a vehicle with independent four wheel steering. While it may not represent the exact vehicle in this project, it is a great basis for the mathematical model of this vehicle.

If the previously stated model is combined with the chosen turning model, then the resulting vehicle model and it's corresponding equation's turn out to be as described in Figure 2.3 and equations 2.14.

These equations, extrapolated from Figure 2.3, form the basic relationship between parameters which can be used to estimate and even regulate how the vehicle is supposed to move. However, how the separate forces are supposed to be evaluated, limiting factors and more relevant equations which are to be used can be found in source [8].

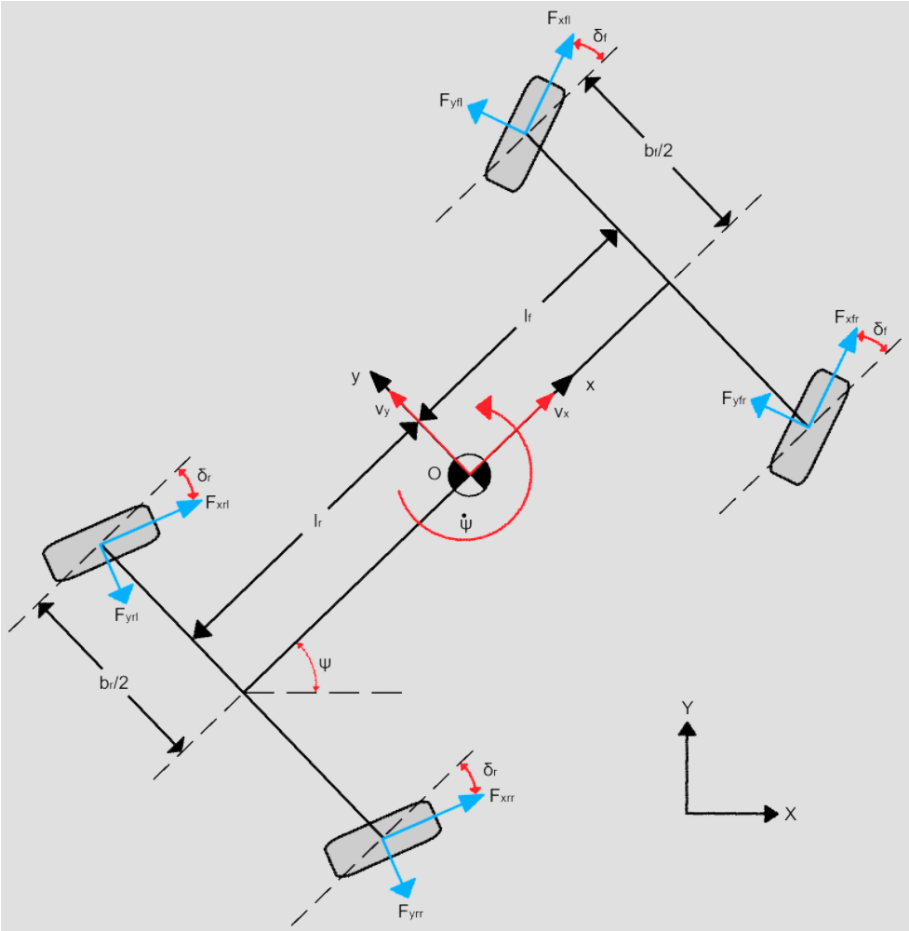

Figure 2.3: The image illustrates the variables defining the vehicle model.

$$\begin{aligned} m\dot{v}_x = mv_y\dot{\psi} &+ (F_{xfl} + F_{xfr})cos(\delta_f) + (F_{xrl} + F_{xrr})cos(\delta_r) \\ &-(F_{yfl} + F_{yfr})sin(\delta_f) - (F_{yrl} + F_{yrr})sin(\delta_r) \end{aligned} \tag{2.14a}$$

$$\begin{aligned} m\dot{v}_y = -mv_x\dot{\psi} &+ (F_{xfl} + F_{xfr})sin(\delta_f) + (F_{xrl} + F_{xrr})sin(\delta_r) \\ &+(F_{yfl} + F_{yfr})cos(\delta_f) + (F_{yrl} + F_{yrr})cos(\delta_r) \end{aligned} \tag{2.14b}$$

$$\begin{aligned} I_z\ddot{\psi} = &\frac{b_f}{2}(-F_{xfl} + F_{xfr})cos(\delta_f) + l_f(F_{xfl} + F_{xfr})sin(\delta_f) \\ &+\frac{b_r}{2}(-F_{xrl} + F_{xrr})cos(\delta_r) - l_r(F_{xrl} + F_{xrr})sin(\delta_r) \\ &+\frac{b_f}{2}(F_{yfl} - F_{yfr})sin(\delta_f) + l_f(F_{yfl} + F_{yfr})cos(\delta_f) \\ &+\frac{b_r}{2}(F_{yrl} - F_{yrr})sin(\delta_r) - l_r(F_{yrl} + F_{yrr})cos(\delta_r) \end{aligned} \tag{2.14c}$$

$$\dot{X} = v_x cos(\psi) - v_y sin(\psi) \tag{2.14d}$$

$$\dot{Y} = v_x sin(\psi) + v_y cos(\psi) \tag{2.14e}$$

$$I_{\omega i}\dot{\omega}_i = T_i - rF_{xi} \tag{2.14f}$$

2.4 Overview of regulation

As stated prior, the point of this project is to make a vehicle, with four wheeled steering capabilities, which can use regulation to, for example, follow a path while remaining stable.

To achieve stability, as defined under "Stability", three specific regulators have been considered, those being the PI, PID and MPC regulators.

2.4.1 PI regulator

The point of a regulator in this project is is to analyze a reference value, for example the goal speed, and trying to get the actual speed to be as close as possible to the goal speed. According to [11], how a PI regulator performs this task is by using multiple specific parameters and variables to formulate a "control signal".

Those are the proportional parameter, K_P, the integrating parameter, K_I, the difference between the current value and goal value, e, the integral between the goal over time and the current value over time, e_I, and the control signal, u.

The proportional parameter has the effect of pushing the current value as close to the target value as possible. It is, however, not enough to always reach the target value, which is why the integrating parameter exists. After getting closer to the target, the integrating parameter's job is to make sure that the difference between the current point and target value is as low as possible by minimizing the integral of the space between. How these parameters preform their task is by affecting the control signal u as shown below:

$$u = K_P e + K_I e_I \tag{2.15}$$

The control signal can, for instance, be the chosen torque for a specific wheel, or the current for a motor. After having been selected, the control signal then gets implemented as the vehicles input which then affects the target value, after which the control signal gets reselected and the regulation starts over again.

2.4.2 PID regulator

It can be found in [11] that a PID regulator works roughly the same as the PI regulator with the difference being the introduction of two new parameters, that being the derivative parameter, K_D, and the derivative of the parameter e over time, e_D.

The derivative parameter makes sure that the derivative of the curve for the vehicle's affected value becomes similar to the derivative of the target values curve. If the current speed of a wheel is equal to and follows it's target speed, then the derivative of the two speeds over time becomes one and the same. However, if the wheel drives

over a pothole, the current speed should logically get smaller, meaning that the derivatives of the curves are no longer the same. The derivative parameter reacts by giving the control signal a boost, as to minimize this derivative difference and to make sure that they become similar as soon as possible. The formulated equation for the control signal is as shown below:

$$u = K_P e + K_I e_I + K_D e_D \tag{2.16}$$

2.4.3 MPC regulator

The model predictive control regulator, MPC regulator, works by taking the previously established vehicle model while constantly trying to predict the optimal parameters for multiple steps in the future, according to [8]. This form of regulation can therefore lead to higher potential stability than the other two regulators since it can consider not only the best regulation for the moment, but also how it may affect the future.

3

Implementation

This section describes how the theories, presented in the previous section, were applied to the prototype design. The considered steering configurations were compared regarding the mechanical complexity and suitability for the project. The selected turning model is then motivated based on this comparison. The section also discusses the considered control strategies and explains why the PI control was chosen for the project.

3.1 Turning dynamics

A positive aspect of using the mathematical model, shown in Figure 2.1, for the steering design is that the math is simple, which means that the calculations and code should be simple to implement. This also means that the movement is easy to predict.

However, the drawbacks are far greater. Considering that the wheels will be the only contacting point between the vehicle and the ground, it would mean that turning would result in the contacting base being reduced, making the car more prone to tipping over and becoming more unstable. It would therefore mean that the steering angle should be significantly reduced.

Another drawback is that of axle collision in the case that the wheelbase is shorter than the track width. Therefore, the proportions of the car have to be restricted so as to mitigate this collision chance.

Regarding the method of separate wheel turning, shown in Figure 2.2, the negatives come from the complexities within the equations. Seeing as there are many different variables affecting the speed results, it would mean that any wrongful estimations could have uncertain effects.

However, this method carries greater positives than negatives. The wheels will most likely not collide as in the previous model, as they stay on the ends of the axles, which are fixed in place. This in turn means that the area of contact should remain roughly the same, in turn making this model more stable than the previous one.

The easiest fix to minimize the complexities of the equations would, according to the theory, be by implementing Ackermann steering in the model. While it does fix the biggest negative about the previous steering model, in Figure 2.2, it also comes with some drawbacks when it comes to four-wheel steering on a tight budget.

One possible method of construction would be to have one motor per wheel for turning. However, this option is too expensive for this project.

Ackermann steering can be achieved with two motors. If one motor controls each side of the vehicle, left & right, it could make both of the wheels turn an equal amount of degrees towards being tangential with the central curve. However, this means that one motor would have to turn two wheels in two different directions while also being on separate axles. This option is possible but requires more planning and careful consideration about the hardware construction, where more mechanical parts have to be added. This can reasonably be considered as counterproductive to the use of steer-by-wire technology, since one of the core advantages of steer-by-wire implementation is to minimize the amount of mechanical components.

This means that the best option for turning, based on the limitations of this project, is the separate wheels model without Ackermann steering. However, the next question is regarding how the equations and analytics of the specific turning model should be implemented.

The idea of implementation is to have the vehicle target speed used in the aforementioned equations to give what the goal values should be for the individual wheels. The responsibility of reaching those goals will be placed on the selected regulation method.

3.2 Regulators

As stated prior in the section "Overview of regulation", the PI regulator works by implementing a control signal that is affected by the difference between the current value and target value, as well as the integral between their respective curves over time. However, what this form of regulation does is that it regulates based on the current values. Therefore, PI regulation should be able to check for good stability in the moment, but it can not guarantee that the currently selected parameters will not negatively affect stability in the future.

The PID regulator works similarly to the PI regulator with the addition of the new derivative parameter. The combination of the parameters K_I and K_D leads to PID regulation being more effective and faster than PI regulation at following the target value. However, quick regulation is not always positive. As stated prior, the derivative parameter gives a boost to the control signal to return to the target value as soon as possible in the moment. The problem with the PI regulator regarding future instability has not been resolved in the PID regulator. Therefore, it could be reasonably concluded that a considerable boost in the speed and/or turn angle, to

get back to target values, is at risk of causing future instability.

Another aspect to consider is human comfort. This project revolves around the construction of an electric car, which humans shall interact with. If the car, for any reason, drives away from the target path, the result would be a huge momentary boost to the control signal, to steer the car back on track. If a human is in the car, that quick turn back may be perceived as terrifying while driving at higher speeds, meaning that the PID implementation may come to infringe on the expected comfort in an electric car.

Therefore, while the PID regulator is faster and more effective than the PI regulator at reaching and maintaining its target value, the speed may be a potential cause for concern, based on the previously established logic, when stability is accounted for.

Regarding the model predictive control, the biggest issue regarding its implementation is the inherent complexity. It takes the vehicle model for multiple time steps, which are affected by the previous steps, and then runs through multiple potential solutions for the model, physics, restrictions and more. The combination with the smallest weight, J, is then selected.

While this seems to be the best solution on paper, its implementation requires more time, effort and knowledge on the subject than anyone in the group has had prior to this bachelor's thesis. Considering the size of the group and the time restriction, this form of regulation may not be feasible for the project.

PI regulation may not be as fast and effective as PID regulation, and it is not nearly as stable as MPC regulation. However, considering the shortcomings of the PID regulator potentially contributing to higher instability and the MPC regulator being too time-consuming for this project, the PI regulator seems to be the better "middle of the road choice". Therefore, PI regulation has been selected for this project.

3.3 Implementation of PI regulation

As stated prior, PI regulation works by inputting multiple parameters and variables and outputting one control variable. The difficult part of PI regulation is acquiring the proportional and integral parameters K_P and K_I. A simple and common way to find these parameters is by Ziegler-Nichols tuning.

According to [12], Ziegler-Nichols for PI regulation works by initially setting K_I to zero and manipulating K_P until the critical gain K_{max} is found. The critical gain can be formulated as the value of K_P at which the closed-loop system exhibits stable, constant and non-dampened signal oscillation. After finding the critical gain, the oscillation period of the constant sine waves can be noted as T_0. After these two parameters have been noted, the resulting parameters can be formulated as follows:

$$K_P = 0.45K_{max} \tag{3.1a}$$

$$K_I = 1.2f_0 = \frac{1.2}{T_0} \tag{3.1b}$$

As previously defined, these parameters and variables are used to formulate the control signal, as shown in Equation 2.15. The issue is, if the difference between the current and target values points, e, or the integration between their curves, e_I, happen to be large, then the result would be that the control signal also becomes large. If the control signal, for example, represents the turning angle for the wheels, then too large values may be impossible if, for example, the turn angle has a maximum reach of $\pm 45^o$.

The solution for this issue is to simply clamp the control signal to minimize the result within the acceptable limits. However, this in turn causes another issue regarding the integration. Since the integral continues to grow even though it has no effect on enlarging the control signal past the limits, it is assumed that the integral may become too powerful once the control signal needs to be lowered, which therefore could lead to slower regulation and in turn, instability. According to [13], this phenomenon is called "integrator windup".

To negate this problem, an "anti-windup system" has to be implemented, which needs to prevent accumulated integration fault when the control signal is trying to reach over its maximum. While multiple anti-windup methods may exist, it has been decided that the optimal way to do so in this project, is simply by not integrating during these specific cases when the desired control signal is not equal to the control signal after clamping.

This method may not be fully efficient and has its drawbacks, primarily in the cases where the saturated control signal is nearly equal to the non-saturated control signal. However, it is a functional method that is assumed to be enough for the scope of simple prototype testing.

4

Components Selection

This section describes the main motors, sensors, and electrical components used in the vehicle. These components were chosen based on the requirements of the prototype, such as providing enough torque for propulsion, enabling steering feedback, and providing the system with suitable voltage levels. Together, these components make it possible for the control system to affect and measure the physical behavior of the vehicle.

When selecting components, both performance and practical aspects were considered. The components had to be compatible with each other while also fitting within the physical limitations and be possible to integrate with the control system. Since the vehicle is a small-scale prototype, availability and simplicity were also important factors.

The first components to be selected were the ones necessary for the vehicle to work, excluding the batteries. Those components are the motors, sensors and control units. After selecting the specific components, a further detailed analysis of the possible connection methods was performed. This affected the selection of batteries, since they had to provide a suitable voltage output for the main components while minimizing the number of required voltage conversion stages. Lastly, the need for power supply stabilization was considered.

The following subsections present the selected components and explain why they were considered suitable for the project.

4.1 Propulsion motors

When choosing the propulsion motors, both the required torque and the supply voltage were considered. The motors had to provide enough torque for the vehicle to accelerate without stalling, while still being small enough for the wheels to be mounted directly on the motor shafts.

To estimate the required motor torque, the vehicle was assumed to accelerate at 0.5 m/s^2. Since the final vehicle had not yet been assembled when the motors

were selected, the total mass was estimated based on the expected mass of the main components and the mechanical design. The required torque per motor was estimated as

$$T_{\text{motor}} = \frac{(ma + C_{\text{rr}} mg)\, r}{n}, \tag{4.1}$$

where m_{est} is the estimated total mass of the vehicle, a is the assumed acceleration, C_{rr} is the rolling resistance coefficient, g is the gravitational acceleration, r is the wheel radius, and n is the number of propulsion motors. The rolling resistance coefficient C_{rr} was approximated as the same as the rolling resistance of a bicycle wheel [14].

Using the estimated vehicle mass of $m_{\text{est}} = 1.5$ kg, together with the variables as $C_{\text{rr}} = 0.02$, $r = 0.08$ m, and $n = 2$, the required torque per motor was calculated using Equation 4.1 as

$$T_{\text{motor}} = \frac{(1.5 \cdot 0.5 + 0.02 \cdot 1.5 \cdot 9.81) \cdot 0.08}{2} = 41.8 \text{ mNm}. \tag{4.2}$$

The final measured mass of the vehicle was 1.2421 kg, which means that the actual required propulsion torque was lower than the design estimate. Using the final mass, the required torque per motor becomes

$$T_{\text{motor,final}} = \frac{(1.2421 \cdot 0.5 + 0.02 \cdot 1.2421 \cdot 9.81) \cdot 0.08}{2} = 34.6 \text{ mNm}. \tag{4.3}$$

The rotary position sensor also adds a small mechanical load to the propulsion motor, since it is driven by a gear mounted on the motor shaft. As the gear ratio between the motor shaft and the sensor shaft is $1 : 1$, the sensor torque was added directly to the required motor torque. According to the data sheet, the sensor has a starting and running torque of 10.6 mNm [15]. Including this load gives

$$T_{\text{req,final}} = T_{\text{motor,final}} + T_{\text{sensor}} = 34.6 + 10.6 = 45.2 \text{ mNm}. \tag{4.4}$$

The selected motor was the MG16B-120-AA-00, which is a 6 V DC geared motor. According to the data sheet, the motor has a rated torque of 60 mNm and a maximum torque of 90 mNm [16], higher during starting. The calculated required torque is therefore below the rated torque when the final vehicle mass and sensor load are used. The motor was also suitable since its rated voltage was close to the available battery supply, and its small size allowed the wheels to be mounted directly on the motor shafts.

4.2 Motor driver

The Digilent PmodDHB1 dual H-Bridge motor driver was chosen because it can drive two DC motors at the same time [17]. This made it suitable for controlling the

two propulsion motors while reducing the number of required components and keeping the electrical system simpler. The motor driver was sufficient since it contains two H-bridges, which allowed the speed and direction of each motor to be controlled individually.

4.3 Rotary position sensors

The AMS22S Non-Contacting Analog Rotary Position Sensor was selected to measure the angular position of the propulsion motor shafts. The sensor provides an analog output signal related to the rotational angle of the shaft [15]. By reading this angle over time, the rotational speed of the wheels could be estimated in real time. This was important since the wheel speed feedback was needed to regulate the propulsion motors during operation.

4.4 Steering motors

The DSS-M15S servos were chosen as steering motors because they provide both position control and analog position feedback. The servos are controlled using a Remote Controlled Pulse Width Modulation (RC PWM) signal, while the feedback signal is an analog voltage between 0 and 3.3 V [18]. This feedback was considered an important feature, since it makes it possible to measure the actual steering angle and use it in the steer-by-wire control system. The operating voltage of the servos is 4.8–7.2 V, which is within the range of the available power supply. At 6 V the servo has a locking torque of 13.5 kg cm, which was considered sufficient for steering the small-scale vehicle.

4.5 Microcontroller

A Teensy 4.1 was selected as the main controller of the vehicle. One of the main reasons for this choice was its high processing capacity, which gives the system enough computational margin for real-time control tasks. This was considered important since the microcontroller has to read sensor values, generate control signals for the actuators, and run the control logic during operation. The Teensy 4.1 was also suitable because it provides several input and output pins which means that one microcontroller was sufficient for the vehicle. This made it possible to interface the microcontroller with the motor driver, steering servos and feedback sensors used in the vehicle [19].

4.6 IMU

A GY-BNO055 IMU was chosen to measure the motion of the vehicle during operation [20]. The IMU was needed to measure accelerations experienced by the vehicle, which could be used to analyze the vehicle behavior during maneuverability tests. This was considered important since the vehicle could be tested in situations where

stability and motion response would be relevant, such as turning and rapid steering maneuvers.

4.7 Batteries

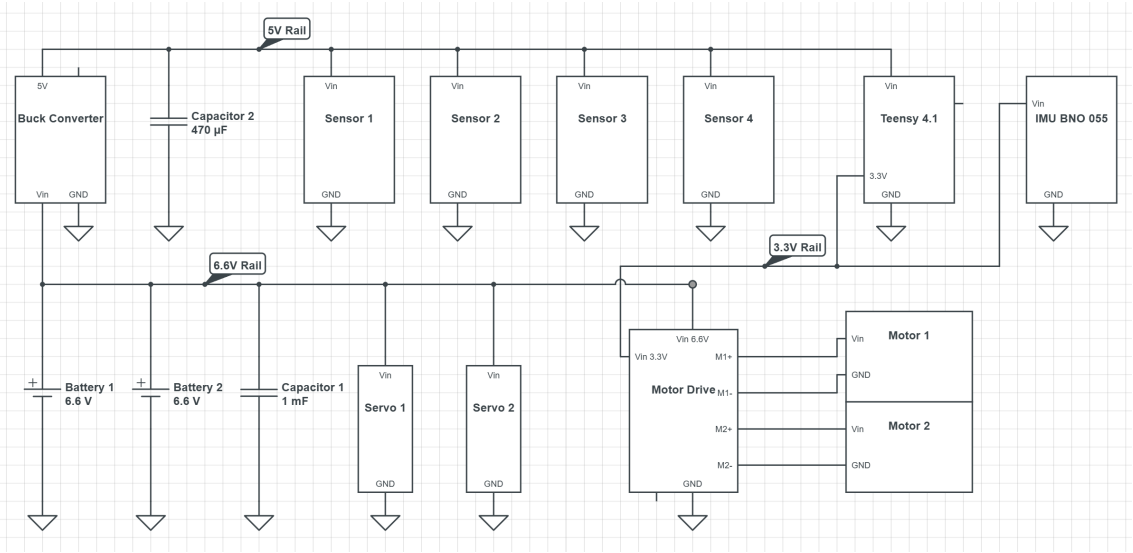

Figure 4.1: Overview of electrical system integration.

NiZn AA batteries were chosen as the main power source for the vehicle because they provided high enough voltage and maximum discharge when connected correctly [21]. By connecting four cells in series, a nominal voltage of 6.6 V was obtained, which was suitable for the motors and other components in the vehicle. Two identical battery packs were used, each consisting of four cells connected in series. The two packs were then connected in parallel to keep the same nominal voltage while increasing the available capacity and operating time of the vehicle. Additionally these batteries were suitable because they are rechargeable while also being in a small form factor.

4.8 Power supply stabilization

A TEC 2-1211WI DC/DC converter was used to create a stable 5 V supply for the microcontroller and sensors [22]. This was needed since these components require a regulated voltage lower than the voltage provided by the batteries.

Capacitors were also added to improve the stability of the power supply. A 1000 μF capacitor was connected in parallel with the higher voltage components to reduce short voltage drops caused by sudden current changes from the motors and servos. A 470 μF capacitor was mounted after the DC/DC converter to help stabilize the 5 V supply and reduce the risk of the Teensy shutting off due to short voltage drops.

5

Development of Vehicle Platform

This section describes how the vehicle prototype was built. It explains the final vehicle design, which mechanical components were manufactured, and how the electrical components were connected. The purpose is to show how the selected components were combined into a physical prototype. The fully built prototype can be seen in Figure 5.1. Additional pictures of the assembled prototype are provided in Appendix A.1.

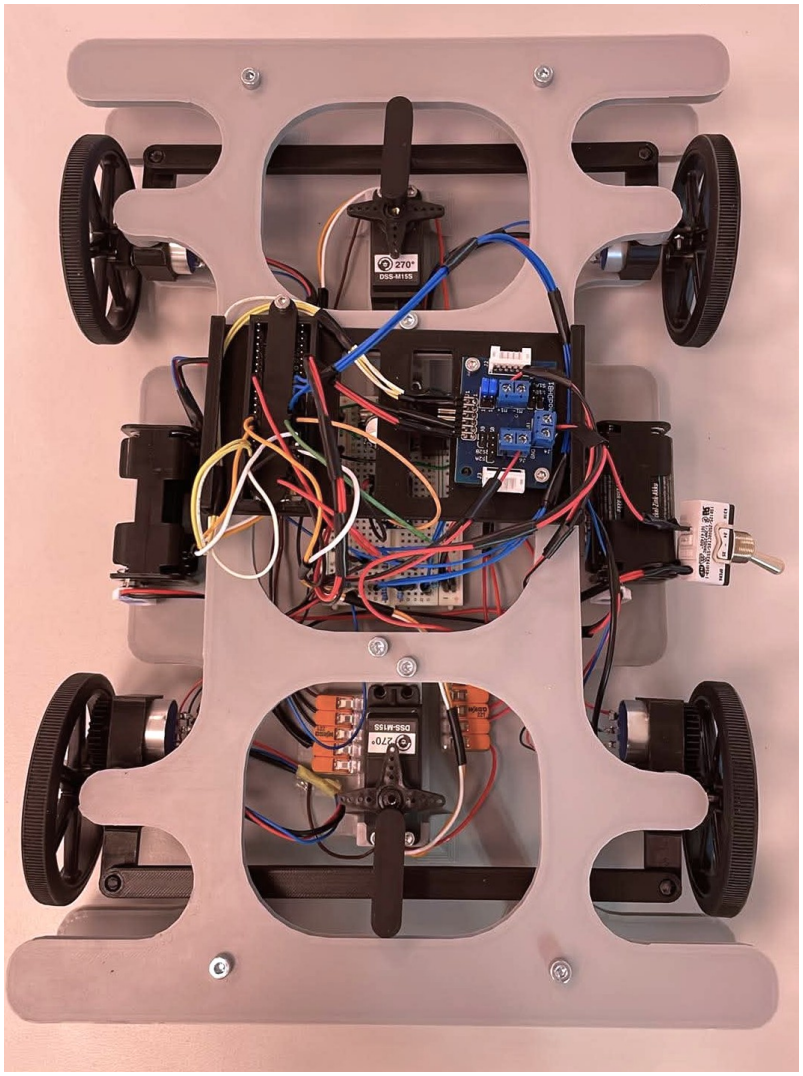

Figure 5.1: The fully assembled prototype vehicle, from above.

5.1 Development of the physical vehicle prototype

Several physical designs were considered during the development of the vehicle prototype. The aim was to find a design that could support four-wheel steering, allow integration of motors and sensors, and still be simple enough to manufacture and assemble within the scope of the project. Cost, ease of assembly, steering range and future modularity were important factors when comparing different design ideas.

Early concepts included a design where each wheel had its own steering and propulsion motor. This would have provided a high level of control, but it also required more components and was considered too expensive for the project. Other concepts were inspired by existing RC car drivetrains, using drive shafts and differentials. These solutions were mechanically possible, but they introduced additional drive-

train losses and limited the steering angle.

The final design was therefore chosen as a compromise between performance, cost, and simplicity. It uses one steering servo for each axle, with mechanical linkages connecting the two wheels on the same axle. Two propulsion motors are mounted on one axle and are directly connected to the wheels, resulting in a two-wheel drive system. This configuration still allows for four-wheel steering, while reducing the number of motors and keeping the drivetrain simple.

The vehicle was designed symmetrically, which allows it to be operated either as front-wheel drive or rear-wheel drive. The modular design of the vehicle makes it possible to add additional propulsion motors in the future with small modifications, which would allow for more advanced experiments. The final design can be seen in Figure 5.2. In the figure, the yellow parts indicate the steering linkages between the wheels on the same axle. The mint green parts show the motor and sensor housings, where the motors are connected to the rotary position sensors using gears. The pink boxes represent the battery packs, and the green square in the middle represents the IMU.

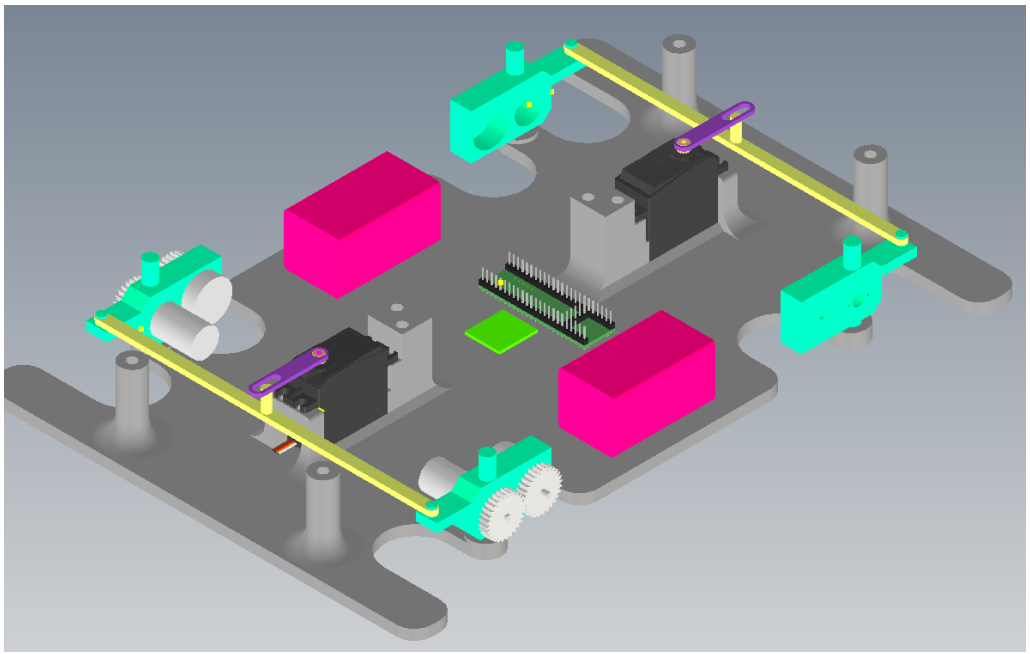

Figure 5.2: Final physical vehicle design with one steering servo per axle and two-wheel drive. Note that the prototype slightly deviates from the CAD model.

5.2 Mechanical design components

Several of the mechanical components were designed and manufactured in-house using 3D printing. This made it possible to adapt the parts to the specific layout of the vehicle and to integrate the motors, sensors and steering mechanism in a compact way. The most important designed parts were the bottom plate, the motor

and sensor housings, the steering linkages, and the top plate.

The bottom plate acts as the main structure of the vehicle. It was designed symmetrically so that the vehicle could be used as front-wheel drive, rear-wheel drive, or four-wheel drive. The symmetrical design therefore allows for testing the vehicle's performance using different drive methods, since the different drivetrains influence the physics of the car. This design decision was made with future development in mind. The plate also includes mounting points for the steering servos, pivot points for the motor/sensor housings, and supports for the top plate. Most of the electronics were placed near the center of the chassis to keep the mass distribution balanced. This placement was also necessary for the IMU, since a placement near the gravitational point gives measurements that better represent the motion of the vehicle.

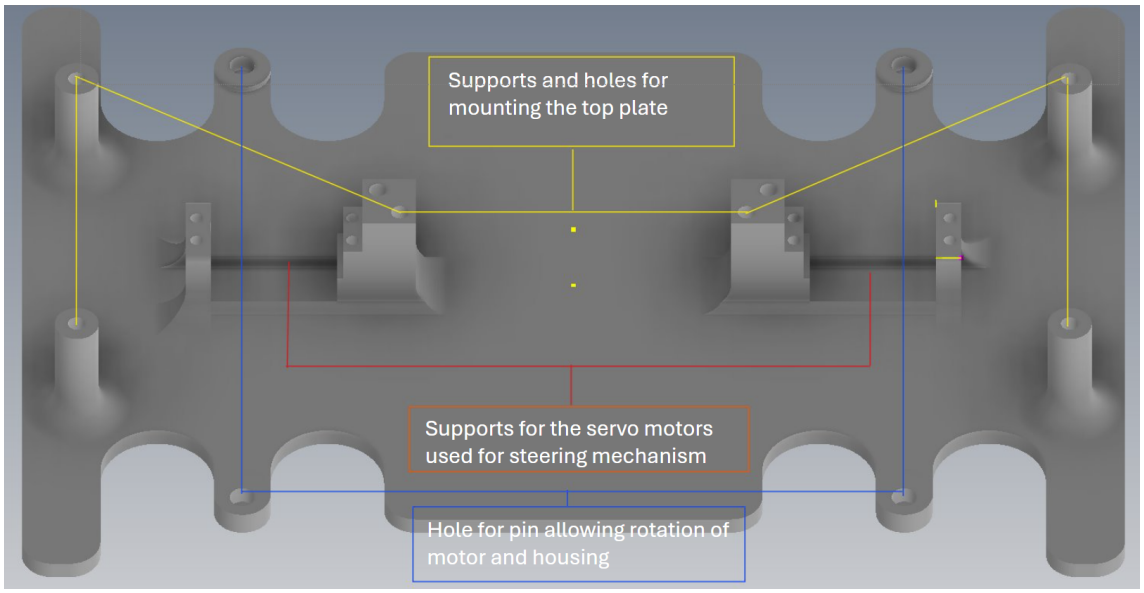

Figure 5.3: Design of the bottom plate with its main features.

The holes marked in blue in Figure 5.3 act as pivot points, allowing the motor/sensor housings to rotate when the wheels are steered. The servo mounts are integrated into the middle of the chassis to keep the servos fixed during steering. Vertical supports with mounting holes are also included to hold a top plate, which protects the electronics and adds stiffness to the chassis.

The motor and sensor housings were designed to keep the propulsion motors and rotary position sensors fixed relative to each other. On the driven axle, each housing contains both a propulsion motor and a rotary position sensor. Two gears were press-fitted, one onto the motor shaft and the other on the sensor shaft. These were connected and allowed the sensor to rotate together with the motor and measure the rotational speed of the driven wheel. The wheel was also mounted to the gear on the motor shaft using screws, which made the motor, gear, and wheel rotate as one unit.

The vehicle is two-wheel driven, but rotary position sensors were mounted on all four wheels. On the non-driven axle, the housings only hold the sensors, Since the wheels are not powered by motors, the wheels was instead connected directly to the sensor shaft. This was done using a 3D-printed clamp, which grips the sensor shaft and holds the wheel in place with screws. This design allowed the rotational speed of all four wheels to be measured, even though only one axle was powered.

Both the motor and sensor housing on the driven axle and the sensor-only housing on the non-driven axle were designed to rotate around the pivot point together with the wheel during steering. This made it possible to combine steering motion with wheel speed measurement in a compact mechanical solution. A more detailed picture of the two different housings can be seen in Figure 5.4.

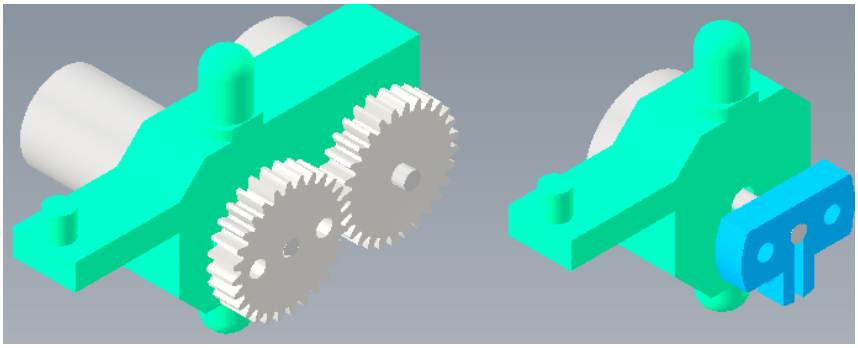

Figure 5.4: The two housing designs. Left: motor and sensor housing for the driven wheels. Right: sensor-only housing for the non-driven wheels.

The steering linkages were used to connect the two wheels on each axle to one steering servo. This reduced the number of servos needed while still allowing both the front and rear axles to be steered. The linkage was designed to give a sufficient steering range while keeping the mechanism simple and easy to assemble.

To make the chassis strong enough, the bottom plate was 3D-printed in Polylactic Acid (PLA) with a 30 % infill. The wall thickness was also increased during slicing to reinforce the structure. This was done to give the pla enough rigidity to handle the loads from the steering and propulsion system, while still keeping the overall weight low. The motor and sensor housings were printed in polyethylene terephthalate glycol (PETG). This material was chosen for the housings since the DC-motors generate heat, and PETG is more heat resistant than PLA.

A top plate was mounted above the bottom plate and it helps keep the the motor and sensor housings in place during operation. The top plate was made symmetrically to distribute the weights evenly. The top plate was manufactured using 3D-printing in PLA, with the same slicing settings as the bottom plate to ensure strength.

5.3 Electrical integration

The electrical components were integrated so that each part of the vehicle recieved the correct supply voltage and could communicate with the main controller. The two battery packs described in Section 4.7 were connected in parallel to form the main 6.6 V supply rail for the vehicle.

The steering servos and the motor driver were supplied directly from the 6.6 V rail. The propulsion motors were not connected directly to the batteries, but were instead connected through the PmodDHB1 motor driver. This was needed since the motor driver controls both the speed and direction of the motors using control signals from the Teensy. The motor driver therefore recieved motor power from the battery rail, while the enable and direction control signals were sent from the Teensy. The Teensy also supplied logic voltage of 3.3 V to drive the logic part of the motor driver.

Some components required a lower and more stable voltage. The DC/DC converter described in Section 4.8 provided a regulated 5 V rail for the Teensy and the rotary position sensors. The IMU was subsequently connected to the Teensy as it required 3.3 V. The stabilization capacitors described previously were connected to the supply rails to reduce sudden voltage drops.

Since the rotary position sensor signal could reach 5 V, voltage dividers were used before connecting them to the Teensy's 0–3.3 V analog inputs.

The Teensy was used as the central controller in the electrical system. It received analog feedback signals from the rotary position sensors and the steering servos. It also sent PWM control signals to the steering servos as well as enable and direction signals to the motor driver. In order to analyze the motion of the vehicle, the Teensy could also recieved data from the IMU. The functional electrical diagram of the vehicle is shown in Figure 5.5.

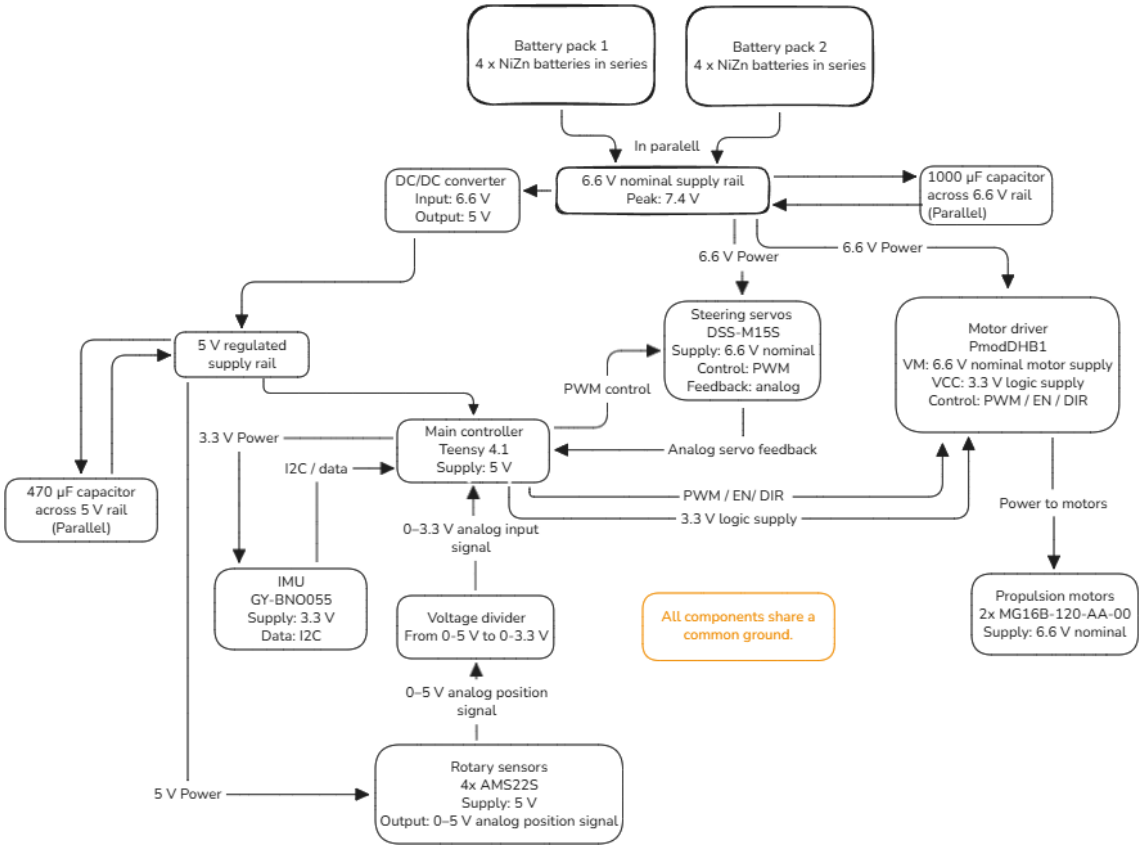

Figure 5.5: Functional electrical diagram of the vehicle, showing the power distribution, voltage regulation, control signals, and feedback signals between the main components.

5.4 Relevant Simulation Parameters

Table 5.1: Measurements, data and parameters used in the simulation.

Parameter	Value	Unit	Description
h	0.001	[s]	Time step
μ	0.7	[1]	Friction constant
g	9.8	$[\frac{m}{s^2}]$	Gravitational acceleration
m	1.2421	[kg]	Vehicle mass
m_w	0.02	[kg]	Wheel mass
r	0.04	[m]	Wheel radius
l_f	0.105	[m]	Distance, center of gravity to front axle
l_r	0.105	[m]	Distance, center of gravity to rear axle
b_f	0.105	[m]	Distance, vehicle symmetry line to front left wheel
b_r	0.105	[m]	Distance, vehicle symmetry line to rear left wheel
h_g	0.04	[m]	Distance, ground to center of gravity
C_α	38	$[\frac{N}{rad}]$	Tyre cornering stiffness
C_κ	67	[N]	Tyre longitudinal stiffness
L_{veh}	0.35	[m]	Length of vehicle
W_{veh}	0.23	[m]	Width of vehicle
T_{rated}	0.06	[Nm]	Rated torque for DC-motors
ω_{rated}	10.47	$[\frac{rad}{s}]$	Rated angular velocity for DC-motors
T_{max}	0.25	[Nm]	Maximum torque for DC-motors
ω_{max}	23.56	$[\frac{rad}{s}]$	Maximum angular velocity for DC-motors
δ_{max}	$\frac{\pi}{4}$	[rad]	Maximum wheel steering angle

The measurements, data and parameters used in the simulation is presented in Table 5.1. Most of the table data can be extrapolated from the aforementioned data sheet's or by measuring the vehicle. However, The tyre cornering stiffness and tyre longitudinal stiffness did not come with any previous data.

The two stiffness's could potentially be extrapolated through testing the vehicle, and later fine tuned until the vehicle works in an optimized manner. However, because of the limited time and scope of the project, this has been deemed as non feasible. The second best option would be to start by assuming their values based on logical data, and then tuning them.

A similar vehicle can be found in [8] where their values are reported to be C_α = 55'000 N/rad and C_κ = 95'000 N. Considering that the force, in newtons, is based partially on the vehicles mass, an initial assumption can be made that the ideal starting values could be the aforementioned values scaled down by the mass difference between the vehicle, in the cited source, and the project prototype. The prototype vehicle has roughly 0.0706% the mass of the inspirational vehicle. This means that the values, scaled down, become as shown in the in Table 5.1.

The issue here is that by scaling down the vehicle, more than just the mass gets affected. So do the forces affecting the vehicle, the tires might be different and there might be other parameters which are unaccounted for. However, this assumption only serves as a starting point to find a rough area to start the tuning. Therefore, while not ideal, this method does its job.

Table 5.2: Measurements, data and parameters used in the simulation.

Parameter	Calculation	Unit	Description
I_z	$m\frac{L_{veh}^2+W_{veh}^2}{12}$	[kgm^2]	Z-axis inertia around vehicle center of gravity
I_{wheel}	$m_w r^2$	[kgm^2]	Wheel rotation inertia
P_{max}	$T_{rated}\omega_{rated}$	[W]	Maximum DC-motor effect
v_{max}	$\omega_{max} r$	$[\frac{m}{s}]$	Maximum wheel speed

The remaining measurements, data and parameters used in the simulation is presented in Table 5.2. These values are only obtainable by having the ones in the previous table. The maximum effect and velocity are easily extrapolated by using common physical relations.

However, the different inertialess have to be assumed based on information regarding the vehicle. When looking at the vehicle from above, Figure 5.1, it's body shape and structure represents what may be considered a rectangle. Therefore, the inertia around the center of gravity's z-axis may be assumed to be that of a rectangle. This relation has a known equation which is formulated in the aforementioned table.

The inertia affecting the wheel's rotation can be formulated as either a plate or a ring. Considering that the greater part of the mass is found in the corners of the wheel with the inner parts being mostly hollow, it seems to be more reasonable to initially assume the inertia to closely resemble that of a standard ring. This too is a known equation and is formulated in the aforementioned table.

5.5 Control software implementation

As Figure 5.6 illustrates, the ideal implementation of the control/regulation software has many variables, parameters and blocks to account for for ideal functionality. The easiest way to analyze the implementation is by focusing on the separate blocks, their functions as well as their respective inputs and outputs. It should also be noted that the selected language for the simulations has been Python, for it's vast number of packages, great simulation qualities and being able to calculate the results of the following blocks.

The block "Turning dynamics" works by taking the target speed of the vehicle and reformulating it into reference values for both wheels. It does so by following the principles described under the section "Turning dynamics - separate wheels". According to the math of the aforementioned section, there might be cases where

the outer wheels of the turn may have a higher velocity than that of the vehicle. Therefore, the tuning dynamics block also has the added feature of restricting the goal velocities of the wheels to stay within acceptable limits.

Another limiting factor is the side slip angle, as defined in the section "Stability". The sideslip angle should be bound within the span of $\pm arctan(0.02\mu g)$, while also being defined as $arctan(\frac{v_y}{v_x})$. Therefore, the system returns a feedback of the current horizontal speed, v_y as to allow for the turning dynamics block to make sure that no goal for the forward velocity makes the side slip angle exceed its bounds.

The blocks regarding the right and left wheel PI implementation work as stated within the section "Implementation of PI regulation". Both of their control signals are the torques which shall be applied on the motorized wheels. They both receive their respective input data containing their respective differences between the target speeds and current speeds, the integral between the goal curve and the actual speed curve, and limiting parameters such as the current angular velocity for the specific wheel.

The specific reason for returning the angular velocities is to analyze the effect output of the motor. The power output of a motor can, in its simplest form, be formulated as the angular velocity of the rotor multiplied by the torque affecting it. This would mean that the maximum control signal, in this case the torque for each wheel, is roughly the maximum effect achievable by the motor divided by the current angular velocity. As a margin of safety, both regulators have a maximum set at 95% of the actual maximum.

The steering regulator uses the difference in the global Y-coordinate over time. This is because the current plan for testing is to make it follow a roughly straight path while being able to turn left and right. The closest comparison to this would be driving down a highway, where the global X-coordinate only moves forward, but the Y-coordinate is allowed to alternate. The regulator, similarly to the others, works by continuously integrating that difference over time while limiting the potential output, in this case, the wheel angle, with some feedback factors.

Those factors are the current yaw rate and the current forces affecting each wheel in directions x and y. It can be assumed that the different forces should have minimal change within a single time step. Therefore, after the PI regulator decides a steering angle, that angle will be inserted with the current forces into equation 2.14c which in turn gives a rough estimation regarding what the potential change in the yaw rate may be over the coming time step. Using that, the regulator block can check if the estimated next yaw rate might exceed its limits, as described in "Stability". After finding a stable steering angle, the block will also check if the steering angle is possible, based on the hardware restrictions.

After selection, all three control signals then get sent to the block, which updates the physical parameters based on the model described in the section "Mathematical

modeling of vehicle dynamics“, and sends the resulting data back into the previously mentioned blocks. Considering that this is a simulation of reality, the final block, which returns the new speed, shall also add a random noise to the signal, which will later need to be filtered. This should in turn make the entire control system and regulation more relevant and show results closely resembling the real world.

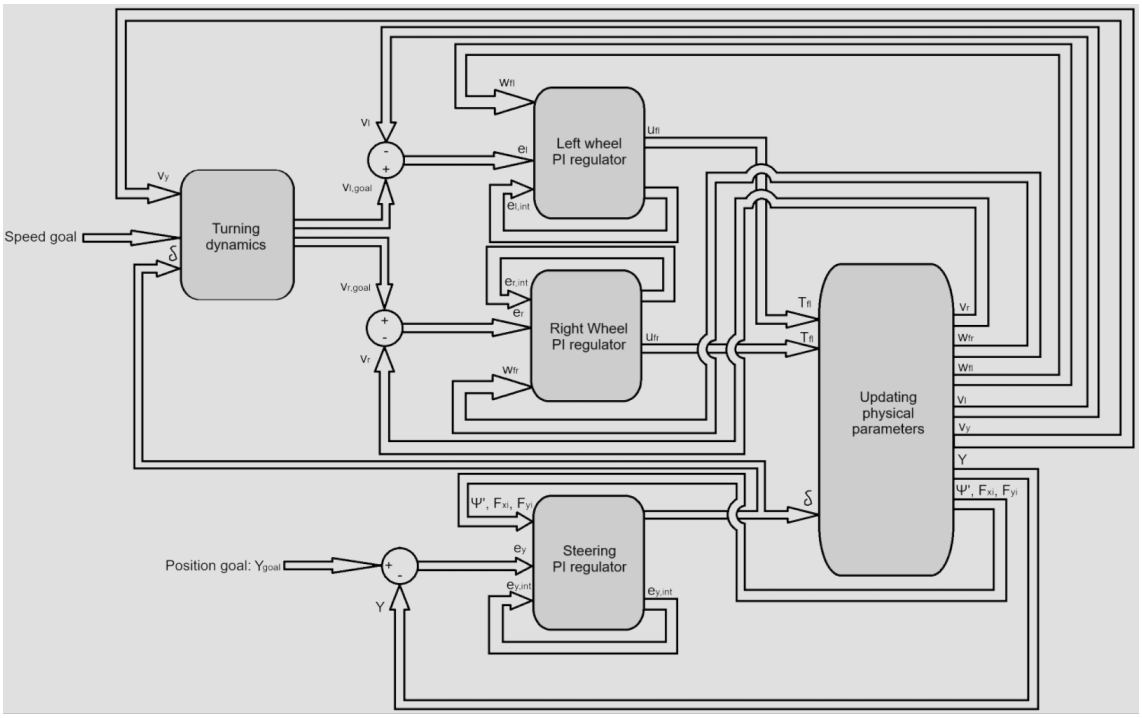

Figure 5.6: The image illustrates full/ideal PI regulation implementation for this project.

6

Results and Discussion

This chapter presents the findings from both the simulations and the physical testing of the steer-by-wire vehicle. The results are presented in graphs and tables. To ensure a clear analysis, a dedicated discussion follows each result.

6.1 Turning Dynamics Simulation

The results for the turning dynamics, during a left turn, are represented in Figure 6.1. What the plot shows is the size of the left wheel velocity as well as the vehicle's actual velocity based as a percentage of the current right wheel velocity and the degree to which the wheels turn. vehicle's

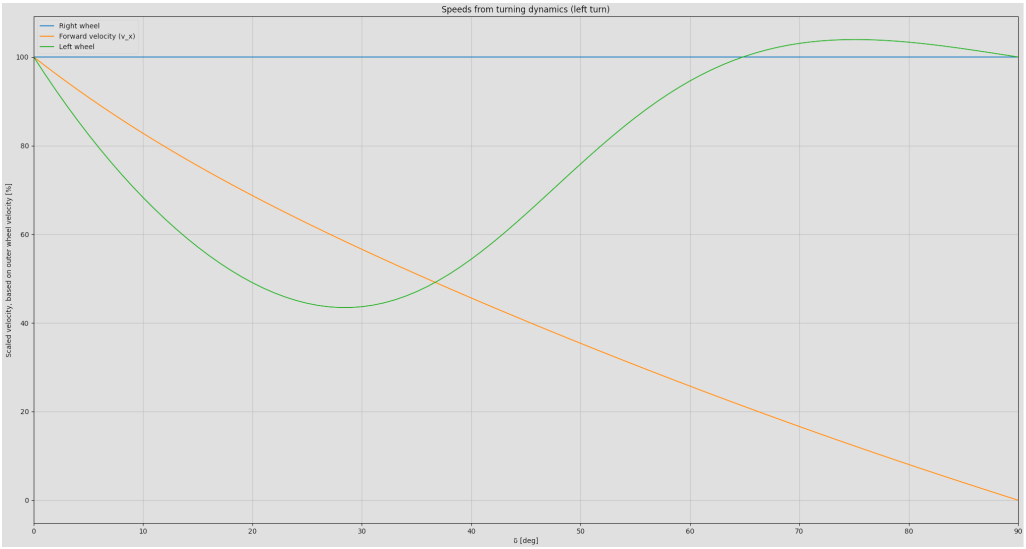

Figure 6.1: Representation of the different speeds, during a left turn, based on the outermost wheel, according to "Turning dynamics - separate wheels".

For instance, the plot shows that all three speeds are equal when the wheel-turning angle is zero degrees. It also shows that, during a ninety-degree turn, the wheels should have the same velocity, while the vehicle velocity is nonexistent.

The results for the turning dynamics, during both left and right turns, are represented in Figure 6.2. This graph indicates that the turning dynamics are the same for both the left and right turns, with the difference being that the right turn's outermost wheels are the left wheels, while the left turn has the right wheels as the outer wheels.

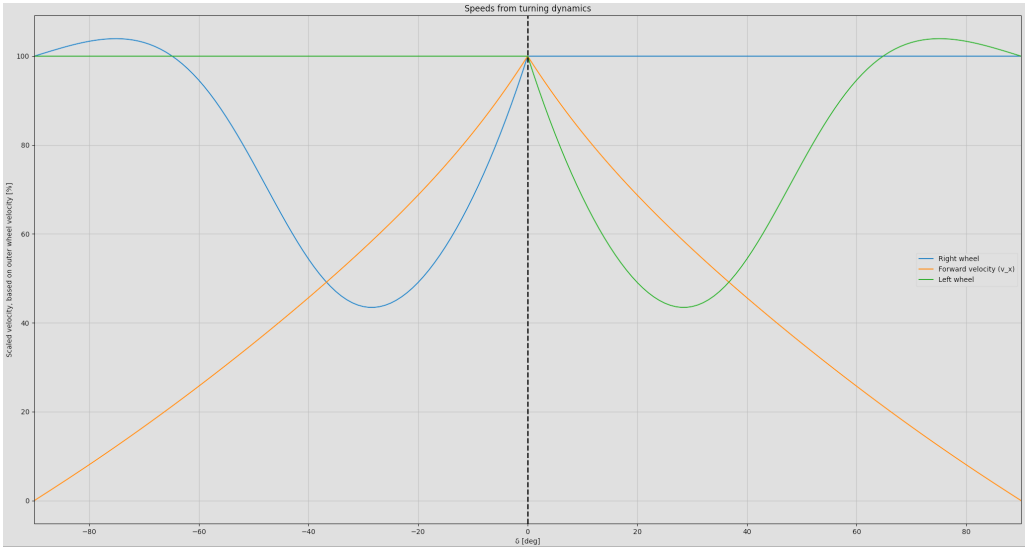

Figure 6.2: Representation of the different speeds, during both left and right turns, based on the outermost wheel, according to "Turning dynamics - separate wheels".

6.2 Discussion of Turning Dynamics Results

The results of the turning dynamics simulation seem reasonable and realistic to what would be expected while driving a vehicle such as this one.

Firstly, the model indicates that the wheel speeds should be exactly the same at two specific steering cases, those being during forward steering and steering at precisely ninety degrees. Logic dictates that if both wheels are directed forward, with the movement directed forward, then both wheels should run at the same velocity.

If the steering angle is set at ninety degrees, then according to the selected model, all wheels should be directed horizontally with the rear wheels facing the exact opposite direction of the front wheels. With this in mind, the equal speed appears to be reasonable, since it would mean that the vehicle rotates around its center of gravity.

Similarly, if the vehicle rotates around its center of gravity without moving in any direction, it would mean that the vehicle does not have a speed in any specific direction, which means that the result of the forward velocity being zero, when the steering angle is set to 90 degrees, is perfectly reasonable.

With these factors in mind, it appears that the mathematical model used to circum-

vent the need for a differential works for the created vehicle. However, it may not be completely accurate.

As stated prior, the rear wheels should reasonably affect the speed, as they have their own dragging forces and non-regulated speeds. However, the dragging forces of the rear wheels are small due to the size of the vehicle and in comparison to the potential force generated by the DC motors. Therefore, the actual speeds may be different from the represented graph. However, the assumption is that the effect should be fairly minimal, and not significant for the software use case.

What the result gives is a response to what the target wheel velocities should be according to the target vehicle velocity and steering angle. However, to achieve the target values set by the results of this simulation is the sole responsibility of the wheel velocity regulators. Therefore, these results are relevant since they are used as input data for the PI wheel velocity regulators.

6.3 PI Controller Simulations

6.3.1 Velocity Control

Using the previously established methods to find the PI parameters resulted in K_{max} = 2 and T_0 = 0.0185, meaning that K_P = 0.9 and $K_I \approx 64.86$. Testing the speed regulation in the forward direction, with the goal of reaching 50% of the maximum speed, resulted in the graphs represented in Figures 6.3 and 6.4.

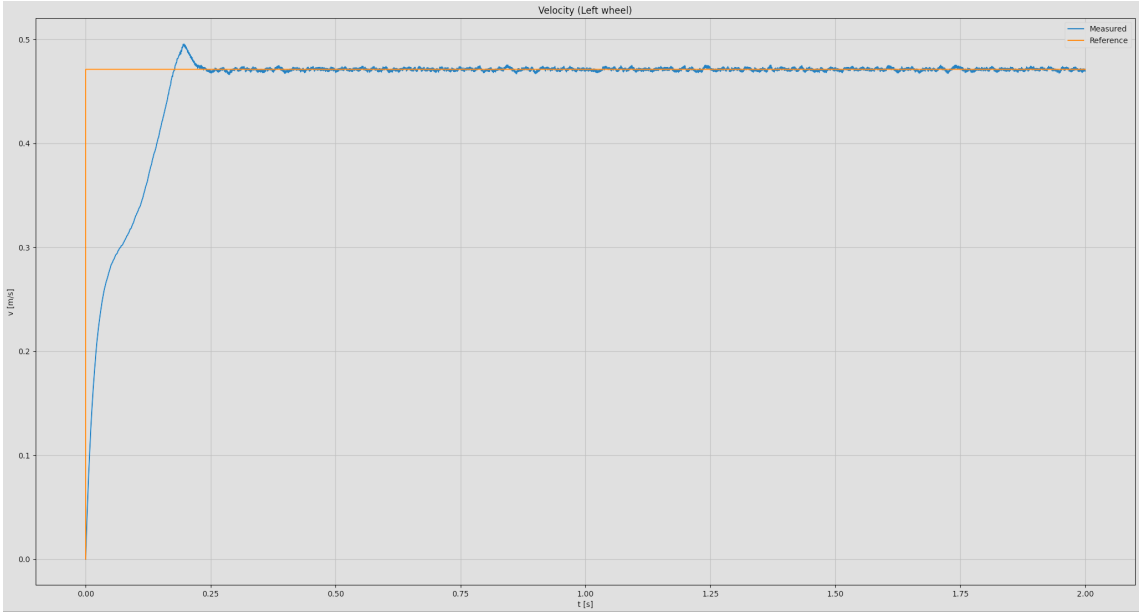

(a) Plot of left wheel velocity

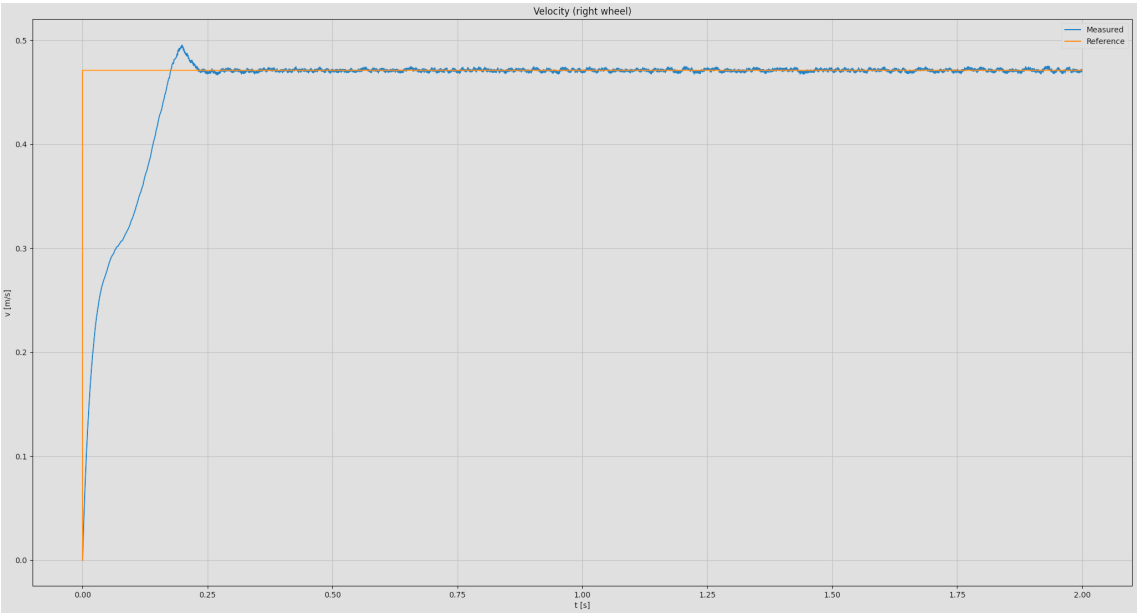

(b) Plot of right wheel velocity

Figure 6.3: Representations of speed regulation when: not turning, goal is 50% of maximum velocity, K_P=0.9 , K_I≈64,86

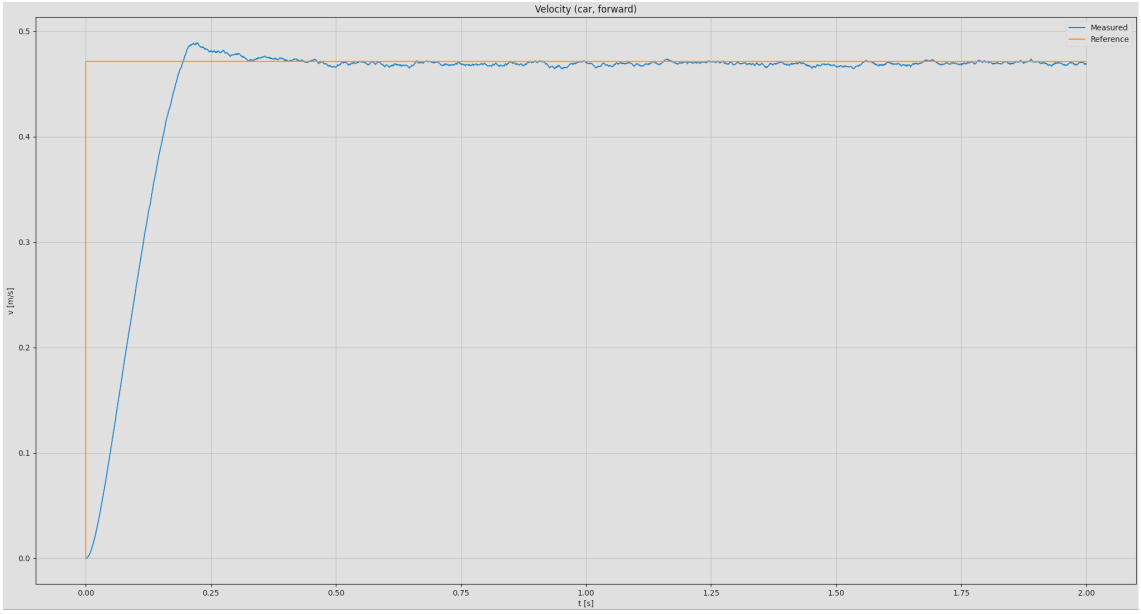

(a) Plot of vehicle velocity in forward direction

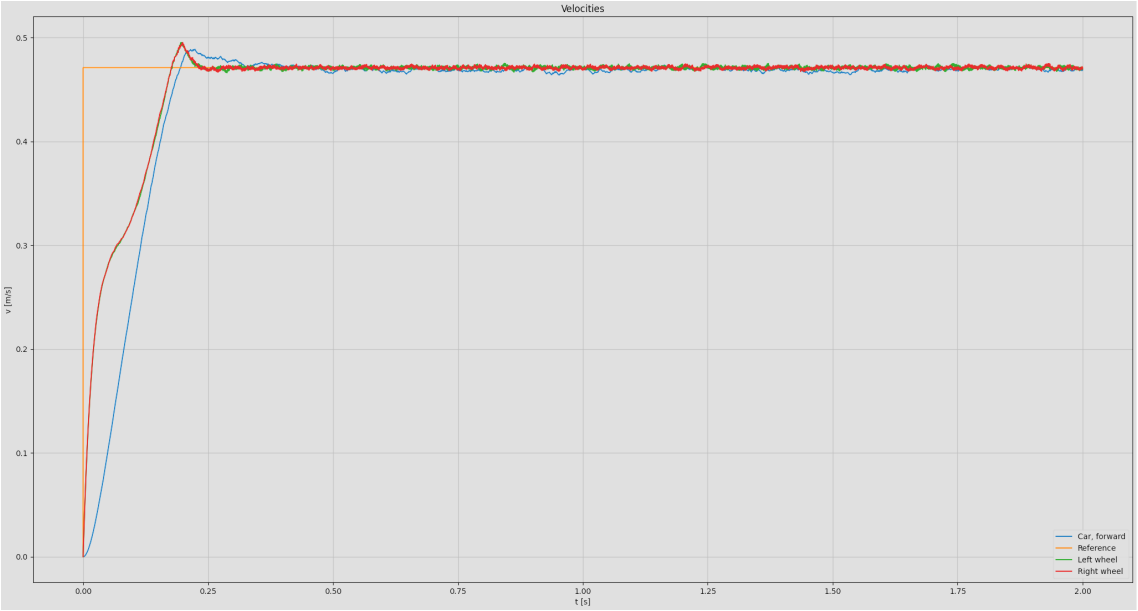

(b) Velocities, overlay

Figure 6.4: Representations of speed regulation when: not turning, goal is 50% of maximum velocity, K_P=0.9 , K_I≈64,86

The graphs show that the three velocities are roughly similar, with the actual vehicle velocity, in forward direction, being slightly slower than the wheel velocities. It is also clear that the great leap from the goal being zero m/s to 50% of the possible maximum lead to the regulators overshooting the target value.

6.3.2 Driving Without Steering

Using the same parameters as in "Velocity Control" resulted in the graphs represented in Figures 6.5 and 6.6. These figures show what happens when placing the vehicle on the ground and allowing for it to move without any steering regulation, where the steering angle remains at zero degrees.

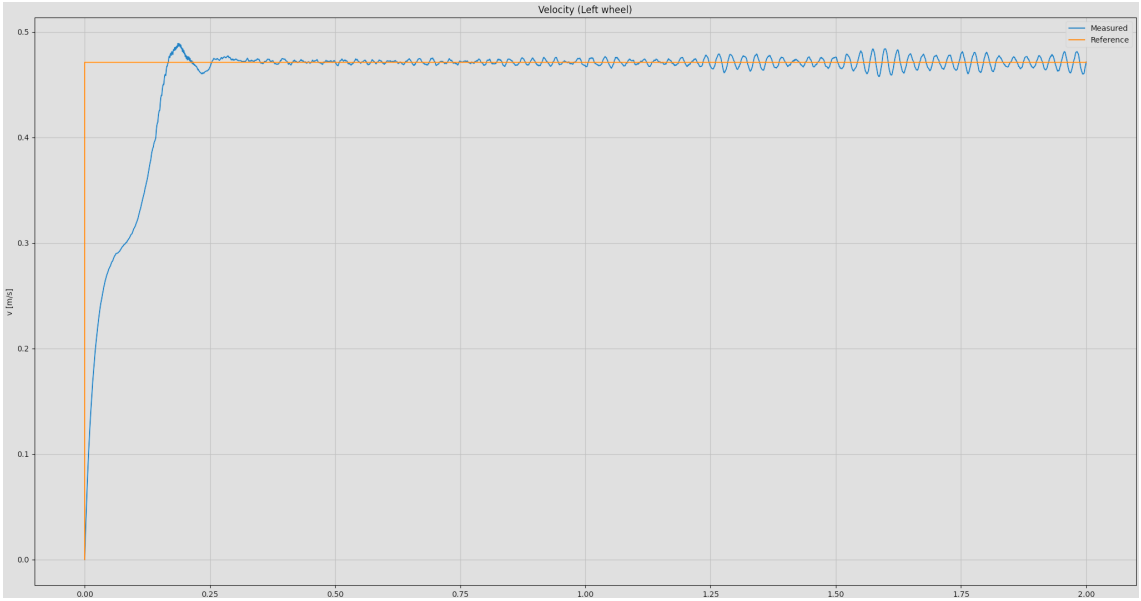

(a) Plot of left wheel velocity

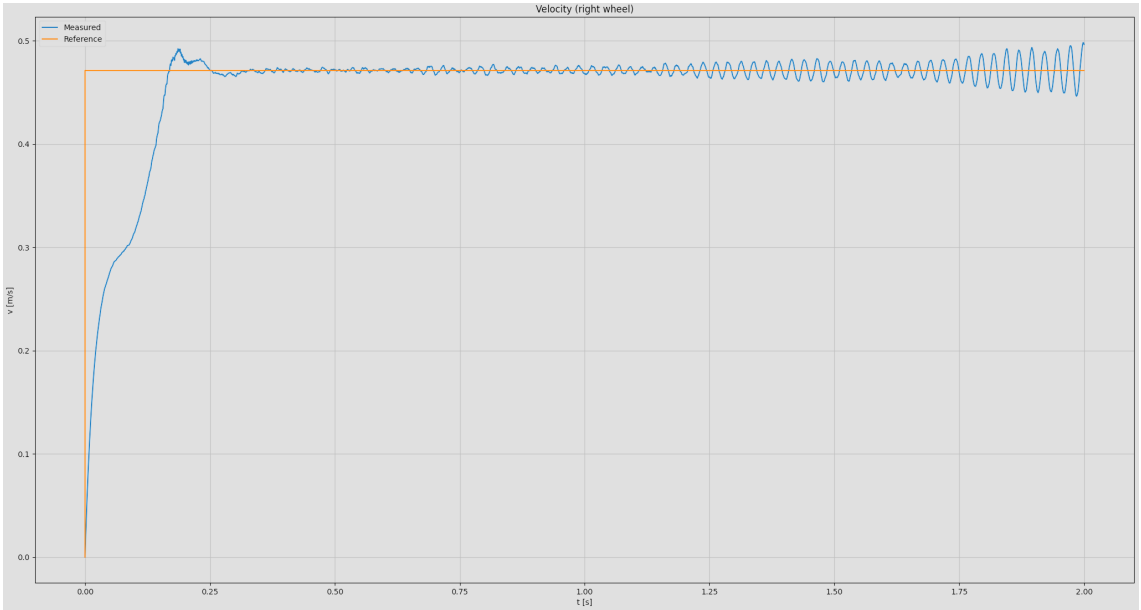

(b) Plot of right wheel velocity

Figure 6.5: Representations of vehicle movement when regulating speed, but not steering.

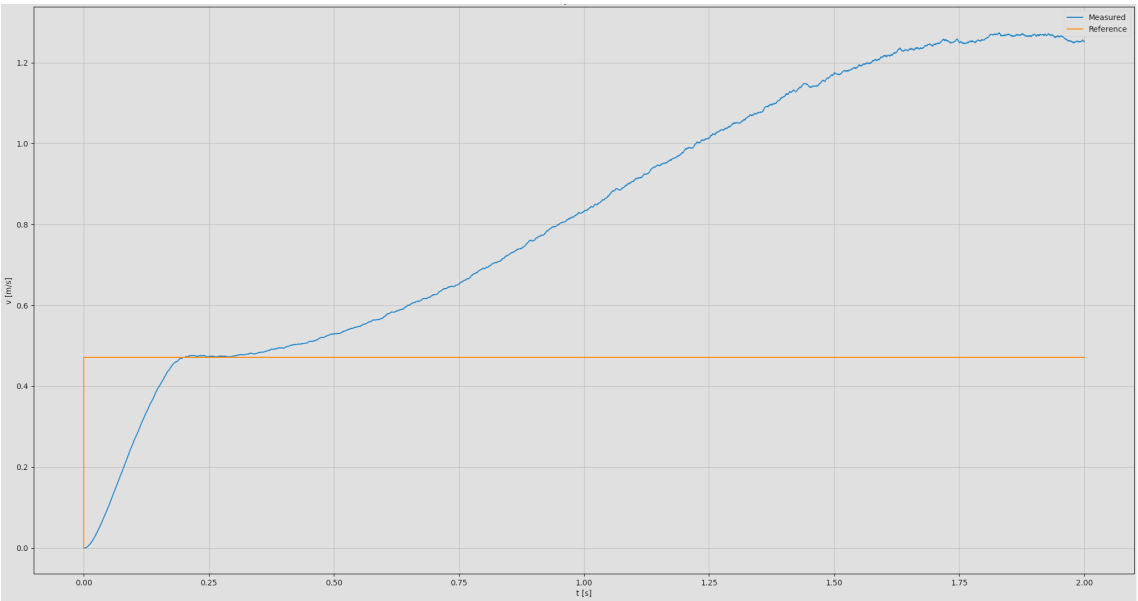

(a) Plot of vehicle velocity in forward direction

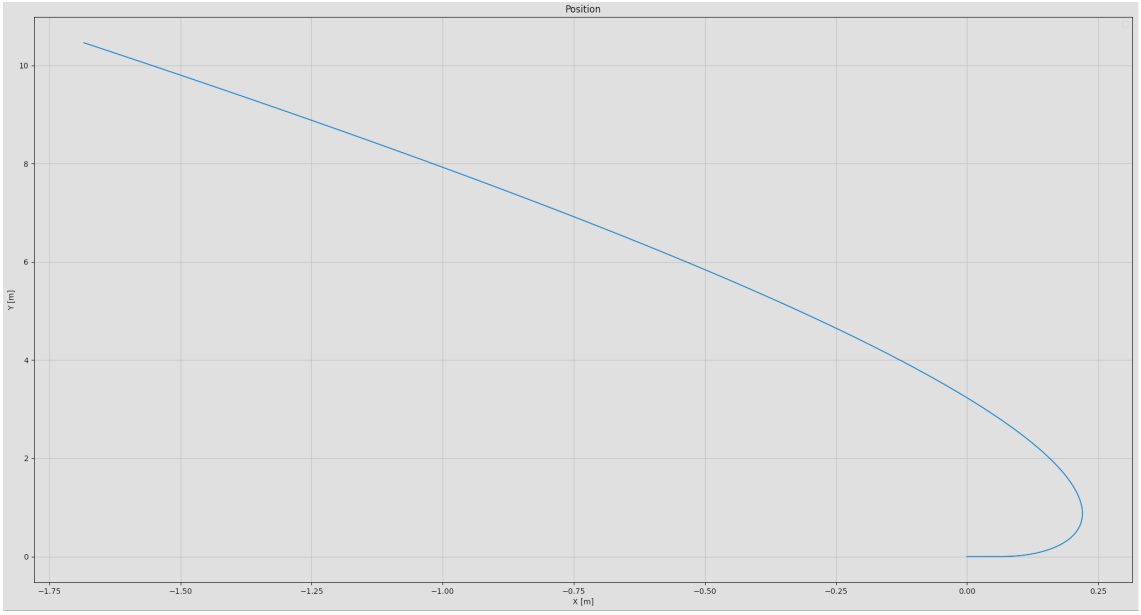

(b) Vehicle movement

Figure 6.6: Representations of vehicle movement when regulating speed, but not steering.

Stress testing of the different parameters in the code has resulted in the finding that the small noise from the sensors leads to the regulators, for the two wheels, outputting slightly different torques. The different torques in turn cause to the wheels to end up with different speeds, which in turn creates a yaw rate. During this process. This in turn causes the vehicle to, over a period of time, become more and more unstable.

6.3.3 Steering Control

The graphs in Figures 6.7 and 6.8 represent the vehicle driving and steering with a simple PI regulator implemented, for the steering. This PI regulator was clearly not finished within the time frame of the project deadline. However, the regulator has been developed to the point that the steering control, at the very least, forces the vehicle to drive towards the right, along with the horizontal X axle. Further fine tuning would be required to perfect the PI steering regulation.

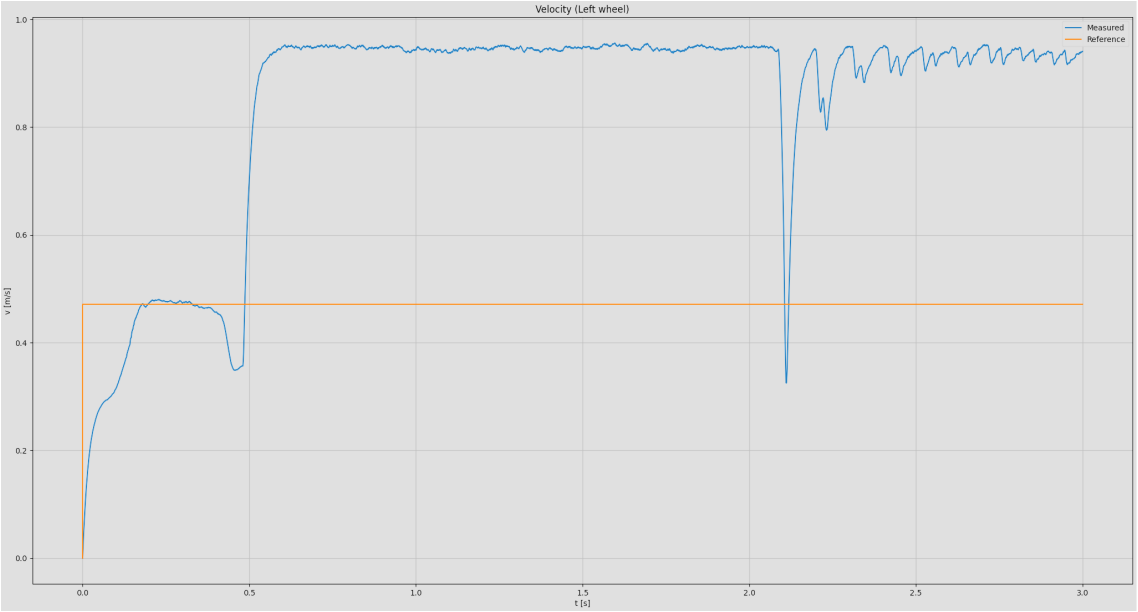

(a) Plot of left wheel velocity

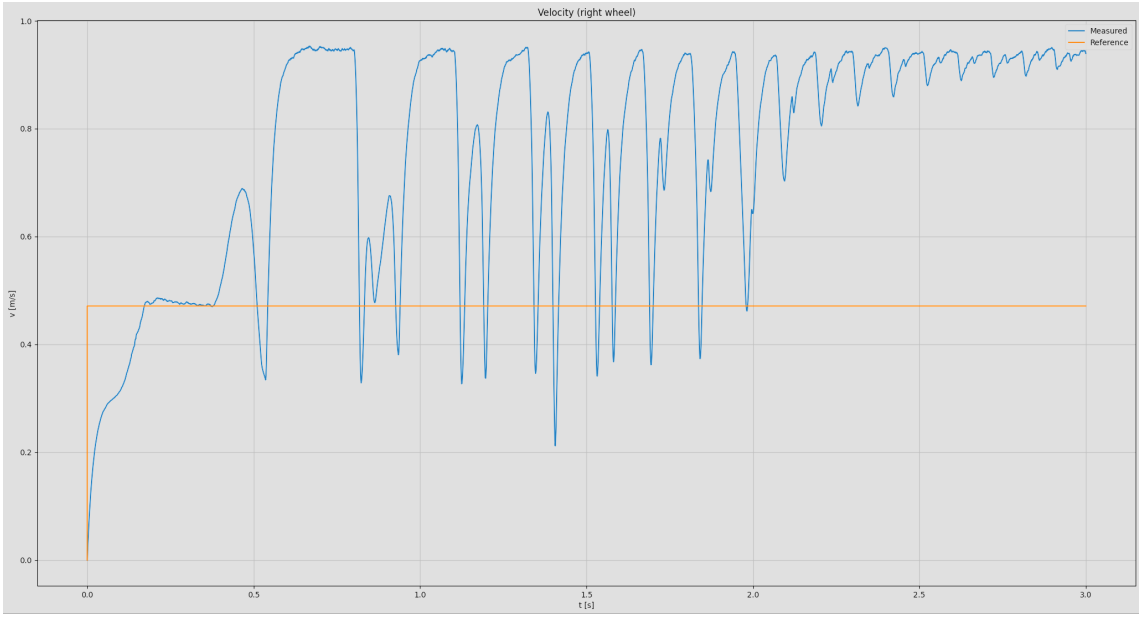

(b) Plot of right wheel velocity

Figure 6.7: Representations of vehicle movement when regulating speed and steering.

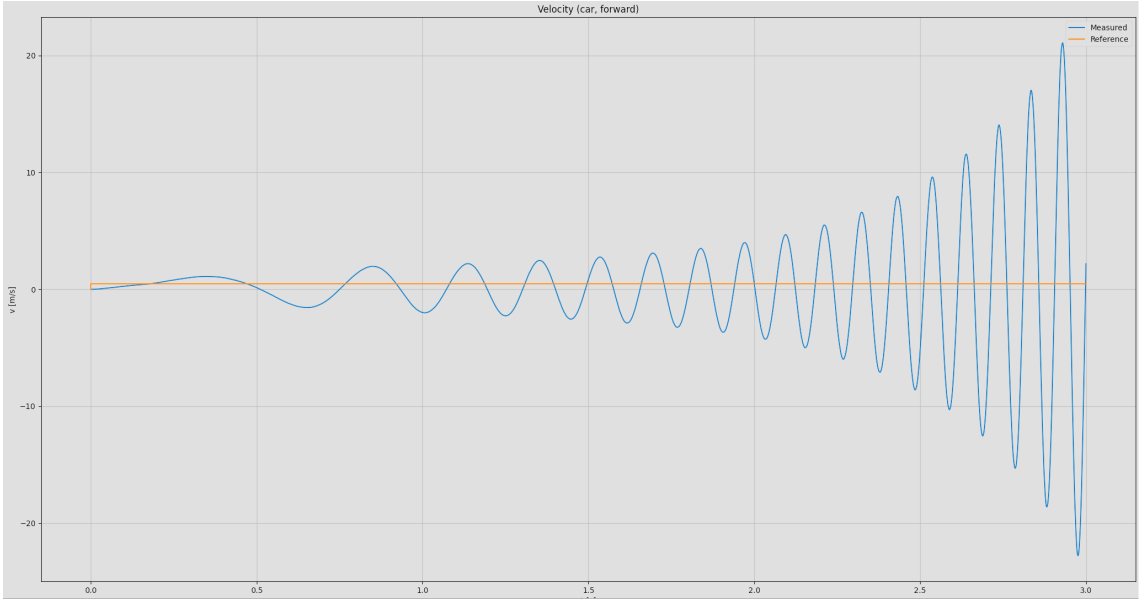

(a) Plot of vehicle velocity in forward direction

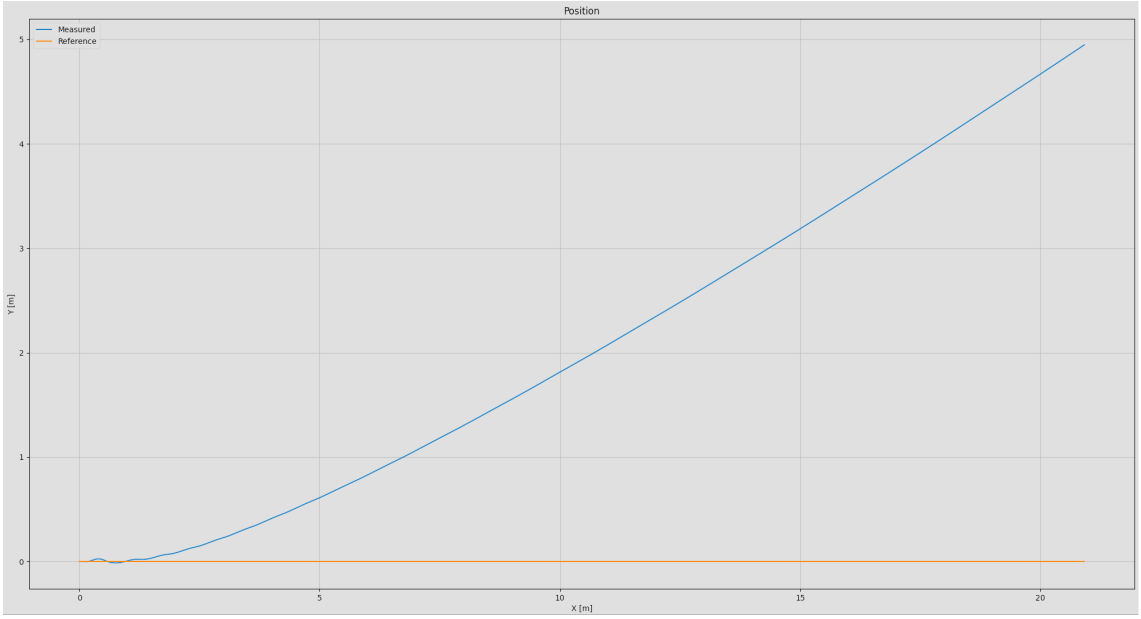

(b) Vehicle movement

Figure 6.8: Representations of vehicle movement when regulating speed and steering.

6.4 Discussion of Simulation Results

According to the result of the velocity control system, the PI regulator should be optimized when the relevant parameters are $K_P = 0.9$ and $K_I \approx 64{,}86$. However, the graphs do show that the regulation overshoots the target value before stabilization. While this may seem odd, it is completely expected.

The reason for the values overshooting is that the system starts integrating from the start of the code. The regulator therefore starts with a huge integral value, e_I, which causes the control signal to be more powerful than needed. This can easily be fixed by adding a delay to the start of the integration sampling, however doing so is unnecessary.

During actual driving, the speed and it's target both start from 0 $\frac{m}{s}$, with the target value growing and shrinking over time, instead of suddenly changing targets from, for example, $0\frac{m}{s}$ to $0.9\frac{m}{s}$. This means that the integration parameter does not start as being excessively large, but instead adapts reasonably over time with the current value trying to follow the target value. Therefore, delaying the integration is not needed.

The regulator could be further developed with methods more precise than the ones used in this project, and a further area of improvement could possibly be the sensor analysis of the speed, where the noise might be reduced further.

Regarding the sensor noise, while it may seem small, it does appear and may be cause for concern, as slight wrongful measurements can result in one motor moving faster than the other, without needing to. This hypothesis is actually a proven result, shown within the graphs in Figures 6.5 and 6.6.

Analyzing the equations under "Mathematical modeling of vehicle dynamics" gives the reason for why the graphs look the way they do. The higher torque on one wheel, caused by the sensor noise, leads to the angular velocities of the wheels to be different. The difference in torque and angular velocities will in turn manipulate the forces affecting each wheel in their respective x and y axle. The forces being different does in turn cause a rise in the yaw rate, leading the vehicle to experience slip. The different forces also affect the total acceleration in the vehicle´s forward direction which in turn affects the vehicle's actual velocity in a way which can not be described by the previous calculations regarding the turning mechanics.

Simply put, the slight difference in the measured velocities caused by sensor noise causes a domino effect of different problems which in turn result in vehicle instability. It is therefore apparent that the result can be used as an example for the importance of noise minimization, or the selection of better sensors. If the project were to reach further development, then this would be an ideal and recommended area of improvement.

However, this happens if the vehicle drives without any steering implementation. If the vehicle yaw rate causes the vehicle to move away from the desired path, then the steering should be able to force the vehicle back to the target position. This is where the steering regulation should step in.

This specific part of the regulation system has not been fully realized due to the limited time frame of the project deadline.As stated in the results, the regulator has

been developed to the point that the steering control, at the very least, forces the vehicle to drive towards the right, along with the horizontal X axle.

If this regulation was to be fully realized, then further fine tuning would be required. However this is simply not possible within the remaining time of the project.

6.5 Physical Prototype Wheel Speed Regulation

Due to hardware-related issues during the integration phase, the complete control strategy developed in the simulation could not be implemented on the physical prototype within the project timeframe. Instead, a reduced control strategy was implemented to test the propulsion motor control of the prototype. This consisted of separate PI controllers for the left and right propulsion motors, using feedback from the rotary position sensors to regulate the rotational speed of each wheel.

Figure 6.9 shows the measured wheel speeds during a constant speed test with a target speed of 80 RPM. During this test, the steering angles were kept fixed in the straight-ahead position, and no trajectory or lateral-deviation measurements were recorded. Both wheels reached the target speed region after the initial acceleration phase. However, the measured speeds oscillated around the reference value with several short-duration deviations visible.

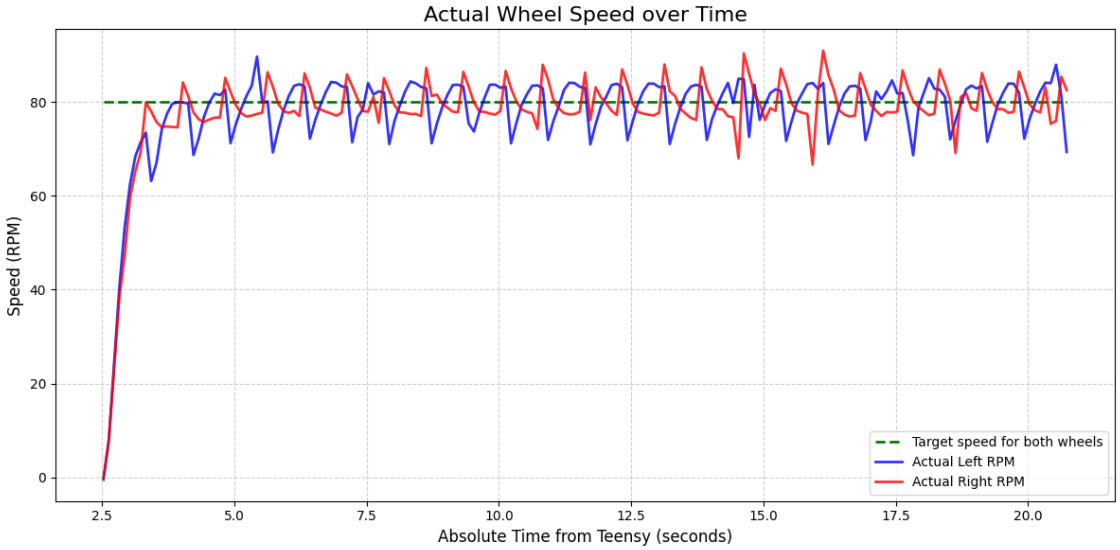

Figure 6.9: Measured wheel speed during PI speed control of the physical prototype. The dashed line shows the target speed of 80 RPM, while the solid lines show the measured rotational speeds of the left and right wheels.

To evaluate the speed regulation more quantitatively, performance metrics were calculated from the same logged wheel-speed data as shown in Figure 6.9. The full test duration was approximately 20 s, and the wheel-speed measurements were logged with an sampling rate of 10 Hz. To exclude the initial acceleration phase,

only the data from approximately $t = 4$ s to $t = 20$ s were used for the calculations. The results are shown in Table 6.1.

Table 6.1: Performance metrics for the PI speed control during the steady-state interval.

Metric	Left wheel	Right wheel
Mean speed [RPM]	79.87	79.92
Mean error [RPM]	-0.13	-0.08
Mean absolute error [RPM]	3.68	3.05
Standard deviation [RPM]	4.48	3.84
Minimum speed [RPM]	68.65	66.67
Maximum speed [RPM]	89.67	90.95
Maximum absolute error [RPM]	11.35	13.33
Samples within ±5 RPM [%]	83.33	83.33
Samples within ±10 RPM [%]	97.62	97.02

The mean speeds were 79.87 RPM for the left wheel and 79.92 RPM for the right wheel, compared to the target value of 80 RPM. This shows that the PI controllers achieved a small average error. The mean absolute errors were 3.68 RPM and 3.05 RPM for the left and right wheels, respectively. This indicates that the average speed tracking was accurate, but that the instantaneous wheel speeds varied around the reference.

The largest absolute deviations were 11.35 RPM for the left wheel and 13.33 RPM for the right wheel. At the same time, 83.33% of the samples for both wheels were within ±5 RPM of the reference, and more than 97% were within ±10 RPM. Overall, the implemented PI controllers provided functional average speed regulation, although the instantaneous wheel speeds showed noticeable variations around the reference.

6.5.1 Physical prototype lane-keeping test

To further investigate the physical prototype's ability to maintain a straight course, a lane-keeping test was performed. The purpose of the test was to evaluate whether the vehicle could drive forward without active steering correction and to quantify its lateral deviation from an intended straight line.

The test was performed by placing the vehicle at the start of a straight reference line, wheels aligned in the forward direction. The left wheels was placed on the line. The vehicle was set to travel at a speed of 80 RPM for 15 seconds without additional steering input. After each run, the lateral deviation was measured as the perpendicular distance from the reference line to the vehicle's left wheels. The measurements was performed manually using a ruler.

To reduce the influence of random variations, the test was repeated 10 times under the same conditions. The measured deviations, together with the mean deviation

are presented in Table 6.2.

Table 6.2: Measured lateral deviation in the physical prototype course-holding test.

Test run	Lateral deviation [cm]
1	52.7
2	3.8
3	117.5
4	69
5	30.2
6	26.8
7	55.8
8	9.1
9	36.2
10	27.5
Mean deviation	42.86
Maximum deviation	117.5

The mean lateral deviation was 42.86 cm, while the maximum deviation from the reference line was 117.5 cm. In 6 out of 10 test runs, the deviation exceeded 30 cm. This indicates that the vehicle did not consistently follow the intended straight path and that noticeable lateral drift occurred.

6.5.2 Discussion of Physical Prototype Results

The results from the PI controller test indicate that the implemented speed control was sufficient to regulate the average wheel speed close to the reference value. However, the measured wheel speeds also showed short-duration deviations. Although the mean speeds of both wheels were close to 80 RPM, these variations show that the instantaneous speed regulation was less consistent than the average values suggest.

The lane-keeping test further supports this observation. Although the PI controller achieved a small average speed error, the physical prototype was not able to consistently maintain a straight course. This indicates that accurate average wheel speed regulation alone was not sufficient to ensure straight-line motion.

One possible explanation is that momentary speed differences between the left and right wheels may have contributed to the observed slip. When one wheel temporarily rotates slightly faster than the other, a yaw moment can be introduced, causing the vehicle to turn slightly.

Several mechanical factors may also have affected the straight-line performance. Tolerances and play between components could influence both the wheel alignment and the steering response. Since most components were manufactured using 3D-printing, manufacturing tolerances may have introduced play between connected

parts. Radial play in the sensor axles may also have caused small movements in the wheels or lateral wheel runout, which would particularly affect the rear wheels, since these are connected directly to the sensor axles. These effects were not investigated separately but could possibly contribute to the observed deviation from the straight line.

Another limitation was the quality of the speed feedback signal. The rotary position sensors measure the angular position, which was then used to estimate the wheel speed. Since the position signal is converted into speed, small variations in the measured angle could have been amplified in the speed estimate. This may have contributed to the noisy feedback signal observed during the constant speed control test.

Electrical effects may also have affected the PI controller. The propulsion motors were controlled using PWM signals, and the motor speed could therefore be influenced by variations in available voltage or current. The available power may vary when other components, such as the servos, are active. This was not measured during the test, but it is a possible source of error.

Despite these possible error sources, the results show that the prototype was able to achieve a steady mean speed. It may also be possible to further improve the speed control, even though speed control would not be sufficient for path following. In order to improve the overall performance of the vehicle, it would be necessary to implement a control algorithm for the steering that works in conjunction with the speed controller. It would also be necessary to implement some form of vehicle state estimation to determine the vehicle's position relative to a reference path. This could be performed with wheel odometry together with the previously established equations for the vehicle dynamics. The simulation results suggest that this type of control approach can work in principle, but it was not validated on the physical prototype within the timeframe of the project.

7

Conclusion

The primary objective for this thesis, to design, construct, and evaluate a modular, small-scale steer-by-wire prototype, was successfully achieved, resulting in a functional vehicle platform that could be used to quantitatively test steer-by-wire control systems.

Simulated tests and analytical data resulted in the extrapolation of individual wheel target values based on the applied vehicle model and physical properties. However, it also resulted in the finding that slight sensor noise can have great effects regarding the separate regulation of the wheels, reaching a point when the resulting torques and forces accumulate unwanted yaw rotation over time. This inadvertently causes the vehicle to drive away from even a straight path, to the point of instability in some cases.

Furthermore, the results from the prototype testing indicated that the mean speed for each wheel can be regulated efficiently using a PI controller. However, the mean absolute errors from the tests were 3.68 RPM and 3.05 RPM for the left and right wheels, respectively. This discrepancy demonstrates that irregular data points can heavily compromise the vehicle's lane-keeping stability. These findings were directly validated in the lane-keeping test, where the vehicle exhibited a mean lateral deviation of 42.86 cm to the left of the straight reference line.

The project resulted in a small-scale vehicle prototype, which can be utilized for future testing of advanced control strategies. Both the simulation and physical testing results indicate that it is possible to achieve efficient wheel speed control using PI controllers.

For further studies, it is recommended to change the regulator implementation to MPC regulation as it is likely to insure greater stability and control. If MPC implementation remains to not be feasible, then the recommendation becomes to further fine tune the system or even to find different solutions which may be more stable. As for the hardware, the greatest improvement would likely come from reducing mechanical tolerances within the steering assembly to minimize system drift.

Bibliography

[1] International Energy Agency, "Global EV outlook 2024." Report, International Energy Agency, Paris, France, 2024. [Online]. Available: `https://www.iea.org/reports/global-ev-outlook-2024`, accessed: 2026-02-06, 2024.

[2] D. L. Anglin, "Automotive steering." *McGraw Hill's AccessScience*, Nov. 2019. doi: 10.1036/1097-8542.064500.

[3] H. Wang *et al.*, "Sliding mode control for steer-by-wire systems with AC motors in road vehicles." *IEEE Transactions on Industrial Electronics*, vol. 61, no. 3, pp. 1596-1611, Mar. 2014. doi:10.1109/TIE.2013.2258296.

[4] H. Zheng, S. Ma, and X. Na, "Design of a variable steering ratio for steer-by-wire vehicle with a joystick." *Advances in Mechanical Engineering*, vol. 9, no. 11, Nov. 2017. doi:10.1177/1687814017730753.

[5] S. Yim, "Comparison among active front, front independent, 4-wheel and 4-wheel independent steering systems for vehicle stability control." *Electronics*, vol. 9, no. 5, p. 798, May. 2020. doi: 10.3390/electronics9050798.

[6] L. Zhai, T. Sun, and J. Wang, "Electronic stability control based on motor driving and braking torque distribution for a four in-wheel motor drive electric vehicle." *IEEE Transactions on Vehicular Technology*, vol. 65, no. 6, pp. 4726-4739, Jun. 2016. doi: 10.1109/TVT.2016.2526663.

[7] J. Zhao and B. Liang, "Self-driving car." *McGraw Hill's AccessScience*, Jun. 2023. doi: 10.1036/1097-8542.613920.

[8] W. Zhang, Z. Wang, L. Drugge, and M. Nybacka, "Evaluating model predictive path following and yaw stability controllers for over-actuated autonomous electric vehicles," *IEEE transactions on vehicular technology*, vol. 69, no. 11, pp. 12807–12821, October. 2020. doi: 10.1109/TVT.2020.3030863.

[9] H. Fischer, "Differential." *McGraw Hill's AccessScience*, Jan. 2020. doi: 10.1036/1097-8542.193400.

[10] W. Zhang, L. Drugge, M. Nybacka, J. Jerrelind, and Z. Wang, "Exploring four-wheel steering for trajectory tracking of autonomous vehicles in critical conditions." in *Advances in Dynamics of Vehicles on Roads and Tracks III*, Ottawa, Canada, 2023, pp. 121-131. [Online]. Available: https://link.springer.com/chapter/10.1007/978-3-031-66968-2_13, Accessed on: 2026-05-13.

[11] W. Bolton, "5 - process controllers." in *Instrumentation and Control Systems*, Oxford, UK: Newnes, 2004. ch. 5, pp. 101-124.

[12] G. Ellis, "Chapter 6 - four types of controllers." in *Control System Design Guide*, 4th ed. Boston, USA: Butterworth-Heinemann, 2012. ch. 6, pp. 97-119.

[13] K. J. Åström and L. Rundqwist, "Integrator windup and how to avoid it." in *Proceedings of the 1989 American Control Conference*, Pittsburgh, PA, USA, 1989, pp. 1693-1698. [Online]. Available: https://ieeexplore.ieee.org/document/4790464, Accessed on: 2026-05-13.

[14] The Engineering ToolBox, "Rolling resistance." 2008. [Online]. Available: https://www.engineeringtoolbox.com/rolling-friction-resistance-d_1303.html (accessed on: 2026-05-10).

[15] Bourns, Riverside, CA, USA, *AMS22S Non-Contacting Analog Rotary Position Sensor*, 2017. [Online]. Available: https://docs.rs-online.com/9ee0/A700000007079082.pdf, Accessed: 10 May 2026.

[16] Nidec Components, Japan, *MG16B DC Geared Motors*, n.d. [Online]. Available: https://docs.rs-online.com/4d87/A700000006965072.pdf, Accessed: 10 May 2026.

[17] Digilent, Pullman, WA, USA, *PmodDHB1™ Reference Manual*, 2016. [Online]. Available: https://docs.rs-online.com/14c9/0900766b816c4a6f.pdf, Accessed: 10 May 2026.

[18] DFRobot, Shanghai, China, *DSS-M15S servos* , 2018. [Online]. Available: https://www.dfrobot.com/wiki/index.php/DSS-M15S_270%C2%B0_15KG_DF_Metal_Servo_with_Analog_Feedback_SKU:_SER00445-3-18, Accessed: 10 May 2026.

[19] PJRC, Sherwood, USA, *Teensy 4.1 Development Board*, n.d. [Online]. Available: https://www.pjrc.com/store/teensy41.html, Accessed: 10 May 2026.

[20] Bosch Sensortec, Reutlingen, Germany, *BNO055 Intelligent 9-axis absolute orientation sensor*, 2021. [Online]. Available: https://www.bosch-sensortec.com/media/boschsensortec/downloads/datasheets/bst-bno055-ds000.pdf, Accessed: 10 May 2026.

[21] ANSMANN AG, Germany, *AA 2500 mWh NiZn Battery*, 2013. [Online]. Available: https://docs.rs-online.com/1f10/A700000012879103.pdf, Accessed: 10 May 2026.

[22] Traco Electronic AG, Baar, Switzerland, *TEC 2WI Series, 2 Watt*, 2018. [Online]. Available: https://docs.rs-online.com/906b/0900766b816edfb7.pdf, Accessed: 10 May 2026.

A

Appendix

A.1 Additional prototype images

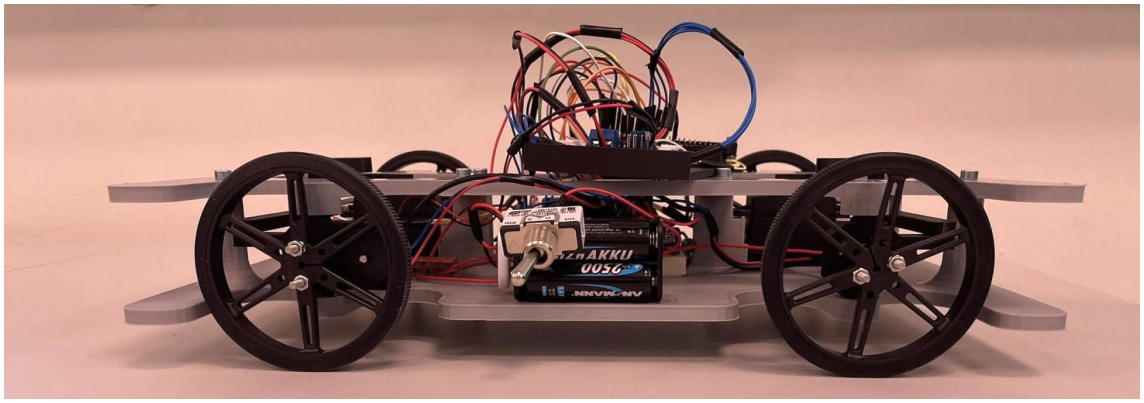

Figure A.1: Side view of the assembled prototype showing the chassis layout.

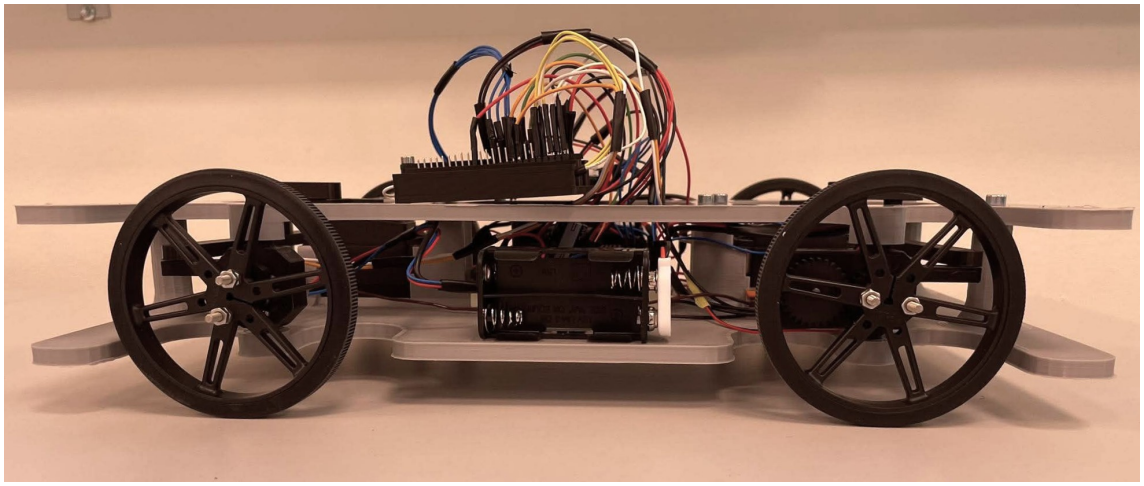

Figure A.2: Side view of the assembled prototype from the opposite side, showing the chassis layout.

DEPARTMENT OF ELECTRICAL ENGINEERING
CHALMERS UNIVERSITY OF TECHNOLOGY
Gothenburg, Sweden
www.chalmers.se

CHALMERS